iCub Whole-body Control through Force Regulation on Rigid Noncoplanar Contacts

Francesco Nori [1], **Silvio Traversaro** [1], **Jorhabib Eljaik** [1], **Francesco Romano** [1], **Andrea Del Prete** [2] **and Daniele Pucci** [1]

[1]*Cognitive Humanoids Laboratory, Fondazione Istituto Italiano di Tecnologia, Robotics Brain and Cognitive Sciences Department, Genoa, Italy.*
[2] *CNRS, LAAS, 7 avenue du colonel Roche, Univ de Toulouse, LAAS, F-31400 Toulouse, France.*

Correspondence*:
Nori Francesco
Cognitive Humanoids Laboratory, Fondazione Istituto Italiano di Tecnologia,
Robotics Brain and Cognitive Sciences Department, Via Morego 30, 16163
Genova, Italy, francesco.nori@iit.it

ABSTRACT

This paper details the implementation of state-of-the-art whole-body control algorithms on the humanoid robot iCub. We regulate the forces between the robot and its surrounding environment to stabilize a desired posture. We assume that the forces and torques are exerted on rigid contacts. The validity of this assumption is guaranteed by constraining the contact forces and torques, e.g., the contact forces must belong to the associated friction cones. The implementation of this control strategy requires the estimation of both joint torques and external forces acting on the robot. We then detail algorithms to obtain these estimates when using a robot with an iCub-like sensor set, i.e. distributed six-axis force-torque sensors and whole-body tactile sensors. A general theory for identifying the robot inertial parameters is also presented. From an actuation standpoint, we show how to implement a joint torque control in the case of DC brushless motors. In addition, the coupling mechanism of the iCub torso is investigated. The soundness of the entire control architecture is validated in a real scenario involving the robot iCub balancing and making contact with both arms.

1 INTRODUCTION

Classical industrial applications employ robots with limited mobility. Consequently, assuming that the robot is firmly attached to the ground, interaction control (e.g. manipulation) is usually achieved separately from whole-body posture control (e.g. balancing). Foreseen applications involve robots with augmented autonomy and physical mobility. Within this novel context, physical interaction influences stability and balance. To allow robots to overcome barriers between interaction and posture control, forthcoming robotics research needs to investigate the principles governing *whole-body coordination* with *contact dynamics*, as these represent important challenges towards achieving robot physical autonomy and will therefore be the focus of the present paper.
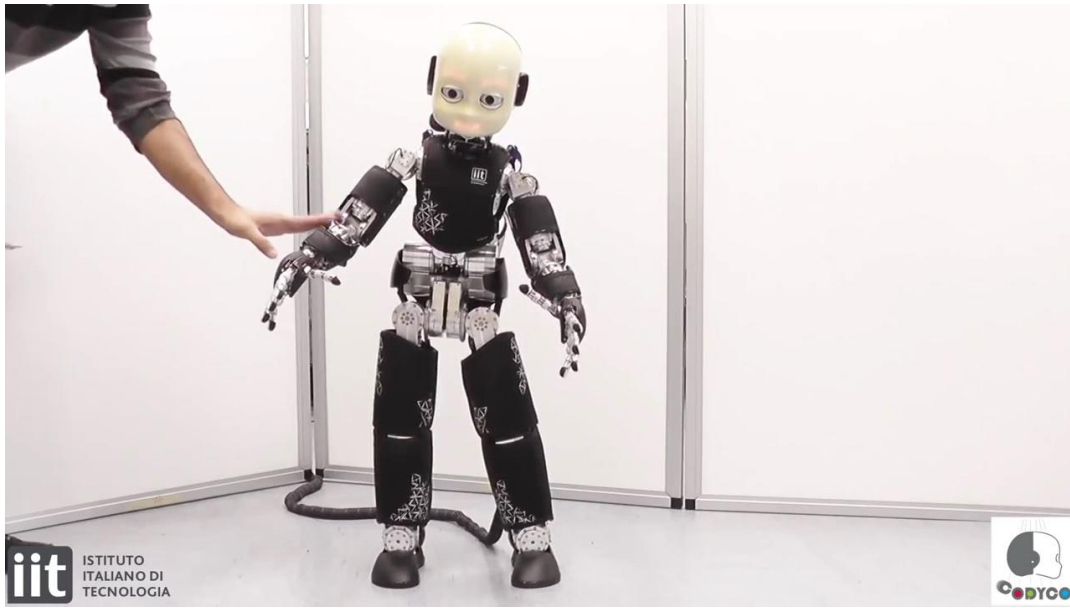
Figure 1. See the video showing the control performances of the control architecture `https://www.youtube.com/watch?v=jaTEbCsFp_M`

26 It is worth recalling that the aforementioned industrial robots have been extensively studied since the
27 early seventies. Robot physical autonomy asks for switching from conventional fixed-base to free-floating
28 robots, whose control has been addressed only during recent years. Free-floating mechanical systems are
29 under actuated and therefore cannot be fully feedback linearized **Spong** (1994). The problem becomes
30 even more complex when these systems are constrained, that is their dynamics are subject to a set of
31 (possibly time-varying) nonlinear constraints. This is the typical case for legged robots, for which motion
32 is constrained by rigid contacts with the ground.

33 The major contribution of this work is the implementation and integration of all the building blocks
34 composing a system for balance and motion control of a humanoid robot. The system includes the low-
35 level joint-torque control, the task-space inverse-dynamics control, the task planner and the estimation of
36 contact forces and joint torques. Even though in recent years other similar systems have been presented
37 **Ott et al.** (2011); **Herzog et al.** (2013), the originality of our contribution lies i) in the specificities of
38 our test platform and ii) in a number of design choices that traded off simplicity of implementation for
39 performances of the control system. In particular:

40 • differently from the other robots, iCub can localize and estimate contact forces on its whole body
41   thanks to its distributed tactile sensors
42 • similarly to the *DLR-Biped* **Ott et al.** (2011), iCub is actuated with DC motors and harmonic drives,
43   but we chose to neglect the gear-box flexibility, which simplified the motor-identification procedure
44   and the low-level torque controller
45 • differently from the above-mentioned platforms, iCub is not equipped with joint-torque sensors, but
46   we designed a method that exploits its internal 6-axis force/torque sensors to estimate the joint torques
47 • all our control loops run at 100 Hz, which is (at least) 10 times slower with respect to **Ott et al.**
48   (2011); **Herzog et al.** (2013)

49 We believe that further investigation will be necessary to thoroughly understand all the consequences of
50 our hardware/software design choices. Nonetheless, these peculiarities make the presented system unique,
51 and for this reason we think it is important to share our results with the robotics community.

The paper is organized as follows: Section 2 reviews the state of the art and motivates our specific choices, with a focus on why we defined postural stability by means of the center of pressure at individual contacts. A counterexample discussed in Section 2.3.3 shows that the commonly-used global center of pressure is not suitable for the scope of our application. Section 3.1 describes the whole-body distributed force and tactile sensors on iCub. These sensors are used to estimate contact forces (Section 3.2.1), internal torques (Section 3.2.2) and to improve the accuracy of the robot's inertial parameters (Section 3.3), while Section 3.4 presents the prioritized contact-force controller. Section 4 discusses the implementation scenario, consisting in controlling the iCub posture and contact forces at both arms and feet. Remarkably, iCub can establish and break contacts at the arms using tactile sensing for both contact detection and localization. Finally, Section 5 draws the conclusions.

2 BACKGOUND

This section reviews previous literature on rigid contacts and their role in whole-body stability. Then we conclude that for the scope of the current paper we need to consider local contact stability as opposed to global stability criteria proposed in previous literature. Section 2.1 makes some general considerations about contacts and Section 2.1.1 gives a characterization of contacts by means of the center of pressure, a point in space that summarizes the effects of distributed forces acting on a rigid body. Section 2.2 focuses on planar unilateral contacts and their stability (Section 2.2.1). This specific type of contacts is associated with a center of pressure that lies on the contact plane (Section 2.2.2). This property is exploited to give necessary and sufficient conditions for the stability of a planar unilateral contact (Section 2.2.3). Section 2.3 reviews previous literature on multiple contacts. In particular, Section 2.3.1 considers the coplanar case, whereas Section 2.3.2 the noncoplanar one. Section 2.3.3 discusses a counterexample to justify our choice of addressing the multiple-contact case without resorting to a global stability criteria as proposed in most of previous approaches. Finally Section 2.4 briefly reviews the state of the art of prioritized task-space inverse dynamics.

2.1 CONTACTS

We consider articulated rigid-body systems under the effects of multiple rigid contacts. In general, a contact can be seen as a continuum of infinitesimal forces acting on the surface of a rigid body. The effect of contact forces will be represented with an equivalent wrench $w_c = (f_c, \mu_c)$, composed by a three-dimensional force and a three-dimensional torque, denoted f_c and μ_c respectively. Considering that a contact exerts infinitesimal forces distributed over a surface, f_c is computed as the integral of infinitesimal forces over the surface. Similarly, μ_c is computed as the integral of the infinitesimal torques due to infinitesimal forces over the surface. The effect of other (noncontact) forces and torques acting on the rigid body, will be denoted $w_o = (f_o, \mu_o)$, being f_o and μ_o the equivalent force and torque (respectively) resulting from all noncontact forces.

2.1.1 Definition of center of pressure (CoP).   Given a rigid body subject to contact forces, we associate a field of pressure to the contact itself. For each contact point, the pressure is defined as the amount of normal force acting per unit area. The center of pressure (CoP) is defined as an application point where the force obtained by the integration of the field of pressures causes an effect that is equivalent to that of the field of pressures itself. *Remark 1:* by definition, pressure accounts only for the normal component of the contact forces acting on the surface of a rigid body. Therefore the CoP comes handy especially when the tangential forces (shear stress) are negligible or do not play a role in the rigid body dynamics (e.g. the effect of tangential forces is compensated by the static friction). Otherwise, the CoP does not represent per-se a full characterization of the forces acting on the system and the effect of tangential forces should be also taken into account. *Remark 2:* at any point in space the effect of a field of pressures can be represented by an equivalent force and an equivalent torque (the integral of infinitesimal forces and

95 torques respectively). Given the above definition, the CoP is an application point where the equivalent
96 torque is null.

97 *2.1.2 Existence of the center of pressure (CoP).*   Given the above definition, we can infer that the CoP
98 sometimes might not exist. As a trivial example, the CoP does not exist when a field of pressure generates
99 a zero net force but a nonzero net torque. Excluding this trivial case, by resorting to the Poinsot theorem it
100 can be shown (see Appendix A) that the CoP is defined if and only if the resulting net torque is orthogonal
101 to the resulting net force. Two relevant cases that satisfy this condition can be identified: field of pressures
102 due to forces lying on a plane (torques orthogonal to the plane) and field of pressures due to forces
103 orthogonal to a plane (torques lying on the plane). The first is a typical example used in aerodynamics
104 (profile of a wing) and the latter is a typical example in the field of humanoid walking (contact with planar
105 surfaces). In any case, the CoP is never uniquely defined and the set of valid CoPs corresponds to the
106 Poinsot axis (see Appendix A.2). In the case of planar contacts, we will uniquely identify the CoP with
107 the intersection between the axis and the planar contact surface as proposed by **Sardain and Bessonnet**
108 (2004).

2.2 PLANAR UNILATERAL CONTACT

109 A particular type of contacts, nominally planar unilateral contacts, has been widely studied to characterize
110 the stability of an articulated rigid-body system while walking on flat terrain. The typical case-study
111 considers a single link (foot) in contact with a flat surface (ground). Proposed stability criteria take into
112 account the fact that while the foot has to be constantly in contact with the ground, the rest of the body is
113 moving and therefore transfers inertial and gravitational forces to the foot. The foot is therefore subject to
114 two sets of wrenches: those due to the contact with the ground (w_c) and those due to the movements of the
115 rest of the body (w_o). For the contact to be stable these forces should balance (see Section 2.2.1). Force
116 balance might not always hold since planar unilateral contacts exert a limited range of forces and torques.
117 Original stability properties were proposed by **Vukobratovic and Juricic** (1969), who introduced the
118 *zero moment point* (ZMP) concept. The ZMP coincides with the unique point on the ground where f_c, μ_c
119 produce zero tangential moments (see Section 2.2.2). As it was pointed out by **Sardain and Bessonnet**
120 (2004), in the case of planar contacts the ZMP coincides with the intersection of the Poinsot axis with
121 the contact plane as defined in Section 2.1.1; the ZMP is therefore a valid CoP. Other stability criteria for
122 planar unilateral contacts have been proposed by **Goswami** (1999) and reviewed in Section 2.2.3.

123 *2.2.1 Definition of stable planar unilateral contact.*   So far we have only discussed about forces
124 generated by contacts. In general, contacts also introduce motion constraints and there is always a duality
125 between contact forces and constrained motion. In the case of rigid contacts, the directions in which
126 motion is constrained are precisely those in which (contact) forces can be exerted as observed by **Murray**
127 **et al.** (1994). In other words, contact forces and possible motions are always orthogonal. From a control
128 point of view it is often desirable that the set of motion constraints does not change over time, since if
129 it does, the control problem becomes harder to solve (see for example literature on hybrid and switching
130 systems). This is the reason why *we say that a contact is stable when the motion constraints induced by*
131 *it do not change over time*. Interestingly, motion constraints are effective on the system only if certain
132 conditions are satisfied. If these conditions are not met (e.g. contact forces violate unilateral constraints or
133 exceed friction cones) contacts are broken and motion constraints are no longer active on the system. It is
134 therefore important to find a set of necessary and sufficient conditions for a contact to constrain always
135 the same motion.

136   In the case of planar unilateral contacts these conditions assume an elegant form that will be presented
137 in Section 2.2.3. The analysis is simplified by observing that planar unilateral contacts impose constraints

138 on all linear and angular motions[1]. Therefore a planar unilateral contact imposes null linear and angular
139 accelerations. By means of the Newton-Euler equations on the contact link, motion constraints are
140 therefore guaranteed if and only if $f_c = -f_o$ and $\mu_c = -\mu_o$. In a sense, deciding whether or not a
141 planar unilateral contact is stable (with the above terminology) corresponds to understanding if a given
142 wrench f_o, μ_o can be compensated by the forces f_c and torques μ_c generated by the given type of contact.
143 If $-f_o, -\mu_o$ lie outside the space of wrenches that a planar unilateral contact can generate, then nonzero
144 accelerations are generated and the contact is broken. The following section shows how to characterize
145 the set of wrenches generated by a planar unilateral contact.

146 *2.2.2 Characterization of the CoP for planar unilateral contacts.*   Given a planar unilateral contact,
147 the set of forces induced by the contact are such that it is always possible to find a point on the plane
148 where the equivalent moment has null tangential components. This point has been named zero moment
149 point (ZMP) by **Vukobratovic and Juricic** (1969). The name is sometimes considered misleading (see
150 for example **Sardain and Bessonnet** (2004)) since at the ZMP the "tipping" (or tangential) moment
151 and not the "total" moment is zeroed. The computation of the zero tipping moment point is relatively
152 straightforward and reformulated in Appendix B.1. In the case of unilateral contacts, the ZMP coincides
153 with the CoP (see **Sardain and Bessonnet** (2004)) and always lies in the convex hull of the contact
154 points as shown by **Wieber** (2002) and in Appendix B.1. It is worth noticing that (in the ZMP context)
155 restricting to tangential moments corresponds (in the CoP context) to neglecting tangential forces (see the
156 first remark in Section 2.1.1).

157 *2.2.3 Characterization of stable planar unilateral contact.*   **Goswami** (1999) pointed out that the ZMP
158 lying within the contact convex hull is not a proper stability measure. He therefore formulated some
159 different statements for the characterization of the stability of planar unilateral contacts. These statements
160 make use of the foot rotation indicator (FRI) which corresponds to the unique zero tipping moment point
161 associated to f_o, μ_o and belonging to the contact plane. The name FRI is misleading since this physical
162 quantity can be associated to any rigid body in contact with a planar surface, regardless of the fact that
163 the body itself is a foot or not. Remarkably, the FRI (differently form the CoP) is not constrained in the
164 contact convex hull because f_o and μ_o are not the result of unilateral contact forces. Other names used in
165 literature for the FRI are fictitious ZMP (FZMP) and computed ZMP (CZMP) used by **Vukobratovic and**
166 **Borovac** (2004) and **Kajita and Espiau** (2008) respectively. If the FRI is not within the contact convex
167 hull, **Goswami** (1999) has shown that a rotation of the rigid link is occurring (i.e. angular acceleration is
168 not identically zero). Viceversa, if the FRI is within the contact convex hull and if frictional constraints are
169 satisfied[2], then the unilateral contact is stable (i.e. the contact link has null accelerations). The complete
170 proof of the latter statement requires some additional considerations which are outside the scope of the
171 present paper. The interested reader should refer to chapter eleven of **Featherstone** (2008).

172 Both the ZMP and the FRI concept have been used by several authors to define a suitable stability margin
173 for balancing an articulated rigid body system. **Hirai et al.** (1998) used the ZMP concept to balance one
174 of the earliest versions of the Honda walking humanoids. **Huang et al.** (2001) adopted a similar concept
175 to define a stability margin tunable by modifying the robot hip motion. **Li et al.** (1993) used the error
176 between a desired and the computed ZMP to learn stable walking. A good reason to prefer the FRI has
177 been pointed out by **Goswami** (1999): given that "the ZMP cannot distinguish between the marginal state
178 of static equilibrium and a complete loss of equilibrium of the foot (in both cases the ZMP is situated at
179 the support boundary), its utility in gait planning is limited. FRI point, on the other hand, may exit the
180 physical boundary of the support polygon and it does so whenever the foot is subjected to a net rotational
181 moment.".

---

[1] Normal linear motion and tangential angular motions are constrained by the unilateral contact forces; tangential linear motions and normal angular motion
are constrained by friction.

[2] The FRI and ZMP (as they have been defined) do not depend neither on the tangential forces nor on the normal moments. However, frictional constraints
depend on these quantities. Therefore, no stability criteria can be formulated using only the FRI and the ZMP quantities. Within this context, it comes with no
surprise that the sufficient condition for contact stability requires tangential forces and normal moments to be within the friction cones of the contact itself.

2.3   MULTIPLE CONTACTS

182 So far we discussed the stability of an articulated rigid body system subject to a single planar unidirectional
183 contact. The stability characterization given by **Goswami** (1999) guarantees contact stability by requiring
184 the FRI to stay inside the support convex hull. In this section we review extensions of this criterium to
185 the case of multiple contacts. Proposed extensions search for some global stability criteria to condense
186 the local stability criteria on individual contacts. Section 2.3.1 considers the simple case of multiple
187 coplanar contacts and the associated global stability criteria, known as global CoP. Section 2.3.2 reviews
188 previous literature on global criteria with multiple noncoplanar contacts. The present section concludes
189 by observing that, for the scope of the present paper, it is mandatory to abandon global criteria and stick
190 to local ones. The conclusion follows from a counterexample, provided in Appendix A.2 and discussed in
191 Section 2.3.3.

192 *2.3.1   Multiple coplanar contacts.*   In this section we consider the case of articulated rigid body systems
193 in contact with a flat surface (typically the ground). Differently from the previous sections, we assume that
194 more than one single rigid body is in contact with the flat ground and therefore we consider a multiple
195 coplanar contacts scenario. Within this context, we distinguish between local CoP (one per each rigid
196 body in contact with the ground) and global CoP (the center of pressure resulting from all rigid bodies
197 in contact). The local CoP of a rigid body has been defined and characterized in Section 2.1.1, 2.2.2
198 and 2.2.3. These definitions and characterizations refer to a single rigid body (e.g. the foot) but can be
199 extended to any rigid body of the articulated system. Computations in this case account only for the
200 contact forces acting on the rigid body itself. Global CoP (GCoP) is instead a quantity associated with
201 the whole articulated system and corresponds to the center of pressure obtained by integrating all contact
202 forces acting on the articulated system. Most of the previous literature does not distinguish between local
203 and global center of pressure but often refer to the latter when characterizing stability during the double
204 support phase of flat terrain walking. Remarkably, the property of the GCoP lying inside the contacts
205 convex hull still holds. This stability criterion has been used by several authors (**Huang et al.** (2001);
206 **Wieber** (2002); **Stonier and Kim** (2006)) to infer stability in flat terrain walking. In particular, **Wieber**
207 (2002) defined a motion to be realizable if and only if the GCoP lies inside the convex hull of contact
208 points. Even though **Popovic and Herr** (2005) questioned the use of the GCoP as a way to guarantee
209 postural stability, associated criteria are at present the most adopted for planning walking trajectories. In
210 Section 2.3.3 we further question the GCoP as a stability criteria, focusing in particular on the scope of
211 the current paper.

212 *2.3.2   Mutiple noncoplanar contacts.*   **Harada et al.** (2003) defined a generalized ZMP (GZMP) and
213 a projected convex hull to formulate stability conditions for a limited class of arm/leg coordination tasks.
214 **Sardain and Bessonnet** (2004) proposed a concept of virtual surface and virtual CoP-ZMP limited to
215 the case of two noncoplanar contacts. In spite of the adopted simplification, authors themselves admit
216 their failure in finding an associated pseudo support-polygon onto which the pseudo-ZMP stays. **Hyon**
217 **et al.** (2007) presented a framework for computing joint torques that optimally distributes forces across
218 multiple contacts; conditions for the CoP to lie within the supporting convex hull are formulated but
219 stability conditions are not formulated with sufficient level of details.

220 *2.3.3   Global versus local CoP.*   In the present paper, we formulate a whole-body postural control
221 which assumes stable contacts. Stability, as defined in Section 2.2.1 guarantees time invariance of
222 motion constraints and avoids the complications of controlling hybrid systems. Necessary and sufficient
223 conditions for stability of individual contacts can be obtained by resorting to the FRI of each contact.
224 Most of previous literature on flat terrain walking postulates the GCoP to lie in the contacts convex hull as
225 a stability criterium. This criterium is a necessary and sufficient condition for a whole body motion to be
226 realizable as pointed out by **Wieber** (2002) (see in particular section 3.2 of his paper). However, it is not
227 a sufficient condition to guarantee stability of all contacts. Appendix B provides a counterexample in the
228 simple case of two coplanar contacts: the GCoP is shown to lie in the contacts convex hull but individual

229 contacts are proven to be unstable. We therefore decide in this paper to stick to local contact stability
230 criteria since no previous global criteria guarantee the stability of all local contacts.

2.4 TASK-SPACE INVERSE DYNAMICS

231 We now briefly review the vast literature on prioritized task-space inverse-dynamics control and we
232 motivate our choices in this regard. **Sentis** (2007) and **Park** (2006) have been pioneers in the control
233 of articulated free-floating rigid bodies exploiting the operational-space framework **Khatib** (1987). More
234 recent approaches have explored the idea of simplifying the system dynamic equations by performing
235 suitable projections onto the null space of the contact forces as proposed by **Righetti et al.** (2011);
236 **Aghili** (2005). While being computationally efficient (i.e. total computation time below 1 ms), all these
237 approaches share a common drawback: contact forces cannot be controlled. As a consequence, stability
238 of the contacts cannot be guaranteed, which may lead the robot to tip over and fall.

239 As opposed to these analytical solutions to the control problem, an alternative numerical approach
240 proposed by **de Lasa et al.** (2010) is to use a Quadratic Programming solver. This allows to include
241 inequality constraints into the problem formulation, which can model control tasks and physical
242 constraints (e.g. joint limits, motor-torque bounds, force friction cones). Even if this technique can
243 guarantee contact stability, solving a cascade of Quadratic Programs with inequality constraints can be
244 critical from a computational standpoint.

245 We decided to take an in-between approach: our framework of choice (see Section 3.4 or **Del Prete et al.**
246 (2014) for details) allows to control the contact forces, but with a computational complexity of the same
247 order of inverse-dynamics-based methods. Compared to optimization-based methods, our implementation
248 does not allow for inequality constraints. To the best of our knowledge, the only real-time implementation
249 of a cascade of Quadratic Programs with inequalities has been tested with a 14-DoF robot on a fast 3.8
250 GHz CPU **Herzog et al.** (2013). We cannot be sure that this method will be fast enough for 26 DoFs and/or
251 a slower CPU. For this reason, while we think that using inequalities could be useful, we postponed it to
252 the (near) future because we know that it demands for an efficient and careful software implementation.

3 MATERIALS & METHODS

253 In this section we present our approach to solve the problem of controlling whole-body posture on
254 multiple rigid planar contacts. We suppose each contact to be planar, but contact planes to be in general
255 noncoplanar. Within this context, the considerations presented in the previous sections justify our choice
256 to abandon the idea of defining a global stability criterion (such as the GCoP). In case of noncoplanar
257 contacts, a global CoP is not even properly defined given that the resulting force and torque might not
258 in general be orthogonal (see Section 2.1.2 and Appendix A.2). In any case, the counterexample in
259 Appendix B.1 suggests to consider multiple local stability criteria instead of a single global one. Local
260 contact stability has been defined in Section 2.2.1 and it has been characterized as a condition for motion
261 constraints to be time invariant. At present, necessary and sufficient conditions for contact stability have
262 been formulated only in the case of planar rigid unilateral contacts (see Section 2.2.3). This is the reason
263 why the scope of the current paper is limited to multiple planar contacts on rigid noncoplanar surfaces.
264 Future extensions of the present work are foreseen in the direction of characterizing contact stability in
265 more general situations.

266 In the rigid and planar contact case, contact stability has been characterized by means of the contact FRI
267 and CoP. Both quantities depend on the wrench (i.e. both force and torque) at the contact point. Assuming
268 that contacts might occur at any point on the robot body, an estimate of the contact wrench might be
269 difficult to obtain if not impossible. Conventional manipulators measure wrenches at the end-effector,
270 where force and torque sensors are placed. Joint torque sensing gives only an incomplete characterization
271 of contact wrenches. The problem can be solved adopting whole-body distributed force/torque (F/T) and
272 tactile sensors as those integrated in the iCub humanoid (Section 3.1). This specific design choice calls for
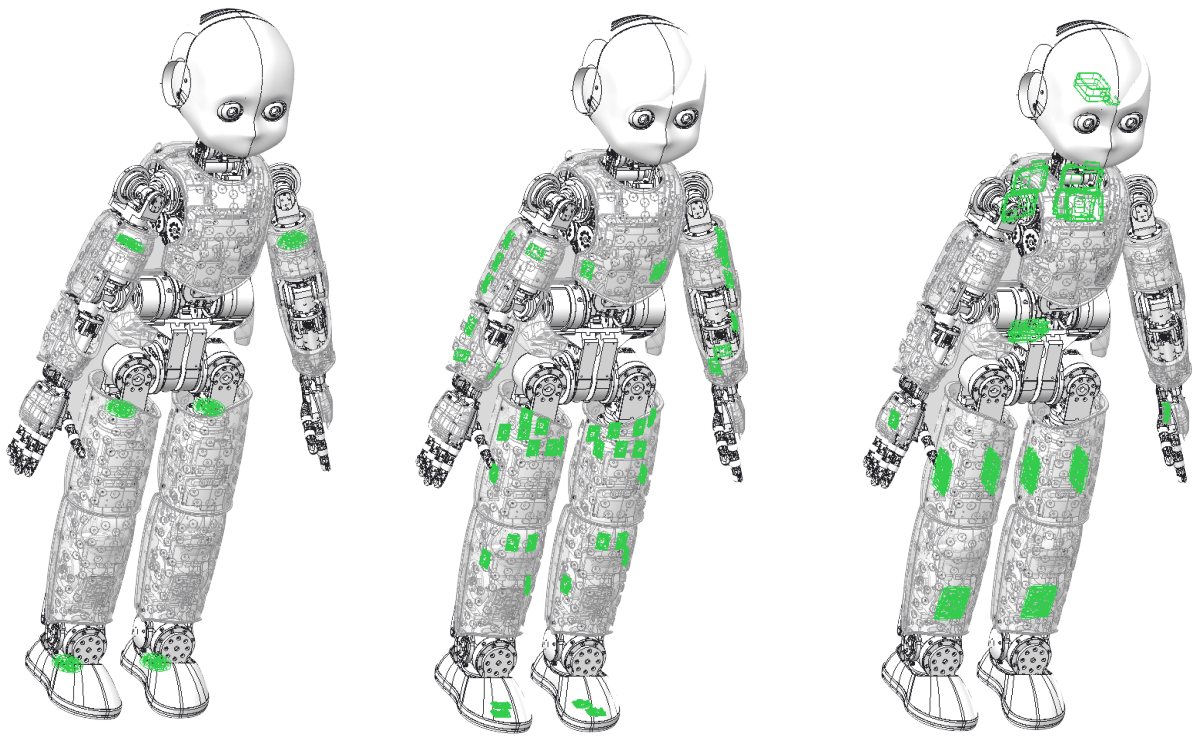
Figure 2. Mechanical schemes of the humanoid robot iCub with force/torque sensors, gyroscopes and accelerometers highlighted in green. **Left**: locations of the six proximal six-axis F/T sensors (legs and arms). **Center**: locations of the skin microcontrollers, which have a 3D accelerometer embedded. **Right**: locations of the motor microcontrollers and the commercial inertial sensor, with the latter having a a 3D gyroscope and a 3D accelerometer embedded.

273 custom algorithms for: contact wrench estimation (Section 3.2.1), internal torques measurement (Section
274 3.2.2) and dynamic model identification (Section 3.3). Whole-body control with multiple noncoplanar
275 contacts is discussed in Section 3.4 and requires all the above custom components for its implementation
276 (Section 4).

3.1 WHOLE-BODY DISTRIBUTED WRENCH AND CONTACT SENSING

277 The platform used to perform experimental tests is the iCub humanoid robot which is extensively
278 described in **Metta et al.** (2010). One of the main features of this system is represented by the large variety
279 of sensors, which include whole-body distributed F/T sensors, accelerometers, gyroscopes (see Fig. 2) and
280 pressure sensitive skin. Furthermore the robot possesses two digital cameras and two microphones. From
281 a mechanical standpoint iCub is 104 cm tall and has 53 degrees of freedom: 6 in the head, 16 in each
282 arm, 3 in the torso and 6 in each leg. All joints but the hands and head are controlled by brushless electric
283 motors coupled with harmonic drive gears. During experimental tests we mainly exploit two kinds of
284 sensors: the F/T sensors and the distributed sensorized skin. The F/T sensor described in **Fumagalli et al.**
285 (2012) is a 6-axis custom-made sensor that is mounted in both iCub's arms between the shoulders and
286 elbows and in both legs between the knees and hip and between the ankles and feet. This solution allows
287 to measure internal reaction forces, which in turn can be exploited to estimate both the internal dynamics
288 and external forces exerted on its limbs. The robot skin **Cannata et al.** (2008) **Maiolino et al.** (2013) is
289 a compliant distributed pressure sensor composed by a flexible printed circuit board (PCB) covered by
290 a layer of three dimensionally structured elastic fabric further enveloped by a thin conductive layer. The
291 PCB is composed by triangular modules of 10 taxels which act as capacitance gauges plus two temperature
292 sensors for drift compensation. In our experiments, iCub's upper body was wrapped with approximately
293 2000 sensors, each foot sole is covered with 250 taxels, while 1080 further sensors are at the last design
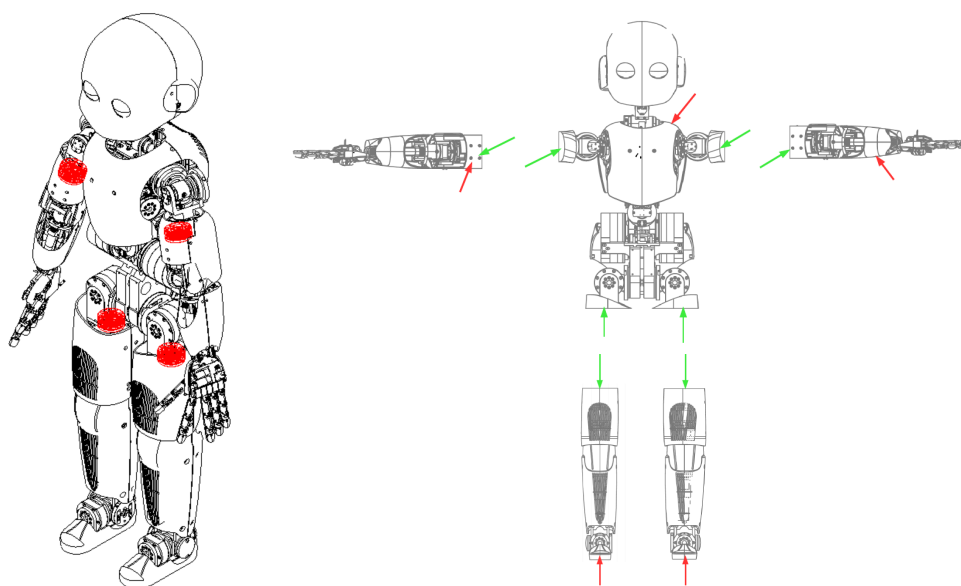
Figure 3. The left picture shows the location of four (out of six) F/T sensors on the iCub humanoid (sensors at the feet are omitted in this picture). The right picture shows the induced iCub kinematic tree partitioning. Each obtained subpart can be considered an independent floating-base structure subject to an external wrench which coincides with the one measured by the F/T sensor (green arrow). Red arrows represent possible location for the unknown external wrenches.

294 and integration stage on the lower body. Each single taxel has 8 bits of resolution, and measurements can
295 be provided as raw data or as thermal drift compensated.

3.2 INTERNAL AND EXTERNAL (CONTACT) WRENCH ESTIMATION

296 **Fumagalli et al.** (2012) proposed a theoretical framework that exploits embedded F/T sensors to
297 estimate internal/external forces acting on floating-base kinematic trees with multiple-branches. From
298 a theoretical point of view, the proposed framework allows to virtually relocate the available F/T sensors
299 anywhere along the kinematic tree. The algorithm consists in performing classical Recursive Newton-
300 Euler algorithm (RNEA) steps with modified boundary conditions, determined by the contact and F/T
301 sensor location. It can be shown that relocation relies solely on inertial parameters, velocities and
302 accelerations of the rigid links in between the real and virtual sensors (see in particular the experimental
303 analysis conducted by **Randazzo et al.** (2011)). The proposed algorithm consists in cutting the floating-
304 base tree at the level of the (embedded) F/T sensors obtaining multiple subtrees as in Fig. 3. Then,
305 each subtree is an independent articulated floating-base structure governed by the Newton-Euler dynamic
306 equations. The F/T sensor, gives a direct measurement of one specific external wrench acting on the
307 structure (green arrows in Fig. 3). Other external wrenches (red arrows in Fig. 3 and Fig. 4) can be
308 estimated with the procedure hereafter described.

309 *3.2.1 Method for estimating external wrenches.* We now describe a method for the estimation of
310 contact wrenches; more details can be found in **Del Prete et al.** (2012). Let us consider a kinematic
311 chain composed by N links, having a F/T sensor at the base (see Fig. 4), where w_i is the wrench (i.e.
312 force and moment) exerted from link i to link $i + 1$, $\ddot{p}_{c_i}$ is the acceleration of the center of mass of link
313 i and m_i is the mass of link i. We know w_0 (i.e. the F/T sensor measurement), the K contact locations
314 $r_{0,ei}, \ldots, r_{0,eK}$ (i.e. the locations where the skin senses contacts), and we want to estimate the K contact
315 wrenches $w_{e1}, \ldots, w_{eK}$. Writing Newton's and Euler's equations for each rigid link and summing up all
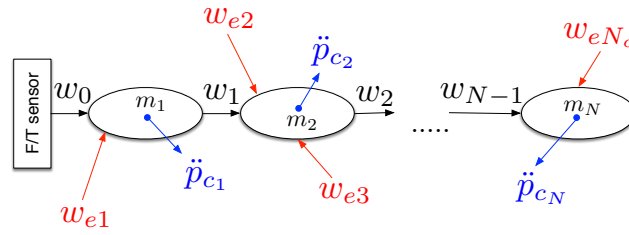316 the N resulting equations we obtain:

Figure 4. Sketch of a kinematic chain with an embedded F/T sensor. Although the sketch refers to a serial chain, the theoretical framework holds also in the case of multiple branches articulated chains (see for example the torso subchain in Fig. 3).

$$f_0 + \sum_{i=1}^{K} f_{ei} = \sum_{i=1}^{N} m_i \ddot{p}_{c_i}, \tag{1}$$

$$\mu_0 + \sum_{i=1}^{K} (\mu_{ei} + r_{0,ei} \times f_{ei}) = \sum_{i=1}^{N} (r_{0,c_i} \times m_i \ddot{p}_{c_i} + I_i^i \dot{\omega}_i + \omega_i \times I_i^i \omega_i), \tag{2}$$

where I_i^i is the inertia of link i, ω_i and $\dot{\omega}_i$ are the angular velocity and acceleration of link i respectively, and r_{0,c_i} is the vector connecting the chain base to the center of mass of link i. Noting that in (1) and (2) the only unknowns are the contact wrenches, the estimation problem may be solved rewriting these equations in matrix form $Ax = b$, where $x \in \mathbb{R}^u$ contains all the u contact unknowns, whereas $A \in \mathbb{R}^{6 \times u}$ and $b \in \mathbb{R}^6$ are completely determined. The equations are constructed taking into account the type of possible contacts among the following three: pure wrench (w_e, 6-dimensional vector corresponding to force and torque); pure force (f_e, 3-dimensional vector corresponding to a pure force and no torque); force norm ($\|f_e\|$, one-dimensional unknown assuming the force to be orthogonal to the contact surface). In the simplest case, only a single contact acts on the sub-chain and the associated pure wrench can be uniquely determined (system of six equations and six unknowns). In other cases, a solution can be obtained with the following least squares procedure. The matrix A is built by attaching columns for each contact according to its type. The columns associated to pure wrenches (A_w), pure forces (A_f) and force norm (A_n) are the following:

$$A_w = \begin{bmatrix} I & 0 \\ S(r_{0,en}) & I \end{bmatrix}, \quad A_f = \begin{bmatrix} I \\ S(r_{0,en}) \end{bmatrix}, \quad A_n = \begin{bmatrix} \hat{u}_n \\ r_{0,en} \times \hat{u}_n \end{bmatrix}.$$

where $S(v) \in \mathbb{R}^{3 \times 3}$ is the skew-symmetric matrix such that $S(v)z = v \times z$, with $\times$ denoting the cross product operator , and $\hat{u}_n$ is the versor of the contact force f_{en}. The matrix A mainly depends on the skin spatial calibration, which can be obtained and refined with the procedure described by **Del Prete et al.** (2011). The 6-dimensional vector b is defined as:

$$b = \begin{bmatrix} f_b \\ \mu_b \end{bmatrix} = \begin{bmatrix} \sum_{i=1}^{N} m_i \ddot{p}_{c_i} - f_0 \\ \sum_{i=1}^{N} (r_{0,c_i} \times m_i \ddot{p}_{c_i} + I_i^i \dot{\omega}_i + \omega_i \times I_i^i \omega_i) - \mu_0 \end{bmatrix}$$

The vector b depends on kinematic quantities which can be derived for the whole-body distributed gyros, accelerometers and encoders. Details on how to estimate these quantities have been detailed by **Fumagalli et al.** (2012). Once A and b have been computed, we can use the equation $Ax = b$ for estimating

external wrenches. The equation defines a unique solution if there is exactly one unknown wrench on the considered subchain. In the case of interest for the present paper, an exact characterization of the interaction wrenches can be obtained if there exists exactly one contact wrench per each of the subchains obtained by the body structure partition induced by the F/T sensor positions (see Fig. 3). In all other situations, an exact estimate cannot be obtained but from a procedural point of view it is preferable to give a reasonable estimate of all the contact wrenches. The solution we adopted consists in computing the minimum norm x^* that minimizes the square error residual:

$$x^* = A^\dagger b$$

330 where $A^\dagger$ is the Moore-Penrose pseudo-inverse of A. The method has been implemented as an extension
331 of the iDyn library[3] and it has been integrated with other software modules to create an efficient software
332 system able to estimate internal and external wrenches of the whole iCub robot.

333 *3.2.2 Method for estimating internal torques.* Once an estimate of external forces is obtained with the
334 method described in Section 3.2.1, internal wrenches can also be estimated with a standard Newton-Euler
335 force propagation recursion. Projection of the internal wrenches on the joint axes provides an estimate
336 of the joint torques τ. A torque controller with joint friction compensation guarantees that each motor
337 provides the desired amount of torque to the joints. In order to improve the torque tracking performance
338 a suitable identification procedure was adopted to estimate the voltage to torque transfer function for
339 each motor. Details are given in the following section together with some details on the dynamic model
340 identification.

3.3 DYNAMIC MODEL ESTIMATION

341 As it was previously pointed out, the technology available in the iCub (nominally, whole-body distributed
342 tactile and F/T sensing) and the estimation algorithm presented in the previous sections allows to
343 simultaneously estimate internal (i.e. joint torques) and external (i.e. contact) forces. The accuracy of
344 the estimates is decisive for the efficacy of the control algorithm that will be described in Section 3.4.
345 A key element to improve the estimation and control accuracy is the availability of a reliable dynamic
346 model (masses, inertias and center of mass positions in equations (1) and (2)). Standard identification
347 procedures do not apply directly and a customization to iCub specific sensor modalities and distributions
348 is necessary. In the following two subsections we describe the solution that we implemented in order to
349 improve dynamic model accuracy (Section 3.3.1) and torque tracking performances (Section 3.3.2).

350 *3.3.1 Dynamic model identification.* The accuracy of the system dynamics (7) is crucial in the
351 proposed control framework since it affects the controller (8) and the internal/external torque estimation
352 procedure described in Section 3.2. Individual dynamic parameters (mass, inertia and center of mass
353 position) of the rigid bodies constituting an articulated chain can be directly obtained from CAD drawings.
354 These parameters are often not sufficiently accurate and standard identification procedures such as those
355 proposed in the handbook of robotics by **Hollerbach et al.** (2008) can be applied in order to improve
356 modeling accuracy. Remarkably, these procedures do not give an estimate of individual parameters but
357 some linear combination of them, known in literature as the *base parameters*. It remains therefore to
358 be clarified if the base parameters suffice to implement the procedure described in Section 3.2.1 to
359 estimate external wrenches. This procedure, written as it is, requires the knowledge of individual dynamic
360 parameters as evident from equations (1) and (2). Additionally, it needs to be verified that also the
361 procedure for estimating internal torques presented in Section 3.2.2 can be reformulated in terms of the
362 base parameters only. Interestingly, it can be shown, resorting to the work by **Ayusawa et al.** (2014) that
363 the base parameters are a subset of those used for both the estimation procedures in Section 3.2.

---

[3] See the software library documentation `http://wiki.icub.org/iCub_documentation/idyn_introduction.html`.

364 *3.3.2 Modeling and representation of the motor transfer function.* Another important component in
365 implementing the control strategy detailed in Section 3.4 is torque control. For the scope of the present
366 paper, it was necessary to implement a model-based controller tuned for each motor. The model assumes
367 that the i-th joint's torque τ_i is proportional (k_t) to the voltage V_i applied to the associated motor, with the
368 additional contribution of some viscous (k_v) and Coulomb (k_c) friction :

$$V_i = k_t\tau_i + (k_{vp}s(\dot{\theta}_i) + k_{vn}s(-\dot{\theta}_i))\dot{\theta}_i + (k_{cp}s(\dot{\theta}_i) + k_{cn}s(-\dot{\theta}_i))\mathrm{sign}(\dot{\theta}_i), \tag{3}$$

369 where $\dot{\theta}_i$ is the motor velocity, $s(x)$ is the step function (1 for $x > 0$, 0 otherwise) and $\mathrm{sign}(x)$ is
370 the sign function (1 for $x > 0$, -1 for $x < 0$, 0 for $x = 0$). Operationally, it was observed quite
371 relevant to distinguish between positive and negative rotations as represented in the model above. We
372 identified the coefficients $k_t, k_{vp}, k_{vn}, k_{cp}, k_{cn}$ for each joint with an automatic procedure implemented in
373 an open-source software module[4]. The motor controller exploits the transmission model and implements
374 the following control strategy:

$$V_i = k_t\left(\tau_i^d - k_p\tilde{\tau}_i - k_i\int\tilde{\tau}_i\mathrm{dt}\right) + [k_{vp}s(\dot{\theta}_i) + k_{vn}s(-\dot{\theta}_i)]\dot{\theta}_i + [k_{cp}s(\dot{\theta}_i) + k_{cn}s(-\dot{\theta}_i)]\tanh(k_s\dot{\theta}_i), \tag{4}$$

375 where $\tanh(k_s\dot{\theta}_i)$ is used to smooth out the sign function, k_s is a user-specified parameter that regulates
376 the smoothing action, and $\tilde{\tau}_i = \tau_i - \tau_i^d$ is the i-th torque tracking error, and $k_p, k_i > 0$ are the low-level
377 control gains. The control objective for the torque controller consists in obtaining $\tau \simeq \tau^d$ and therefore
378 the controller will make the assumption that the commanded value τ_i^d is perfectly tracked by the torque
379 controller. Also, observe that there is no derivative term in the parenthesis on the right hand side of (4). In
380 fact, the measurement of $\dot{\tilde{\tau}}_i$ is noisy and unreliable at the current state of the iCub's measuring devices.

381 *3.3.3 Differential joint torque and motion coupling.* Specific care was posed in controlling the torques
382 at joints actuated with a differential mechanism. As an example, we consider here the torso roll, pitch and
383 yaw joint represented in Fig. 5. In particular, define $q \in \mathbb{R}^3$ the vector of the joint angles Corresponding to
384 the torso yaw, the torso roll, and torso pitch degree of freedom. Also, by abusing notation, define $\theta \in \mathbb{R}^3$
385 as the angles between the stator and the rotor of the motors 0B4M0, 0B3M0, 0B3M1. Then, a simple
386 analysis leads to the following relationship :

$$\dot{q} = T\dot{\theta}, \qquad T =: \begin{bmatrix} \frac{r}{R} & \frac{r}{2R} & \frac{r}{2R} \\ 0 & 0.5 & 0.5 \\ 0 & -0.5 & 0.5 \end{bmatrix}, \tag{5}$$

387 where r and R are the radius of the pulleys sketched in Fig. 5. The above matrix T is obtained
388 by combining a classical differential coupling between pitch and yaw (first two rows) with a more
389 complicated coupling with the roll motion (third row, see Fig. 6). Defining τ_q to be the link torques
390 and τ_θ the motor torques, the coupling induced on torques can be easily obtained by imposing the equality
391 between link and motor powers:

$$\dot{q}^\top\tau_q = \dot{\theta}^\top\tau_\theta \quad \forall\dot{q},\dot{\theta} \qquad \Rightarrow \quad \tau_q = T^{-\top}\tau_\theta \quad \text{with} \quad T^{-\top} := \begin{bmatrix} \frac{R}{r} & 0 & 0 \\ -1 & 1 & 1 \\ 0 & -1 & 1 \end{bmatrix}. \tag{6}$$

392 In the case of coupled joints, the transformation matrix T is used in both (3) and (4) which hold
393 at the motor level. Since position ($\dot{q}$) and torque (τ) feedback is available at the joint level, suitable

---

[4] https://github.com/robotology/codyco-modules/tree/master/src/modules/motorFrictionIdentification
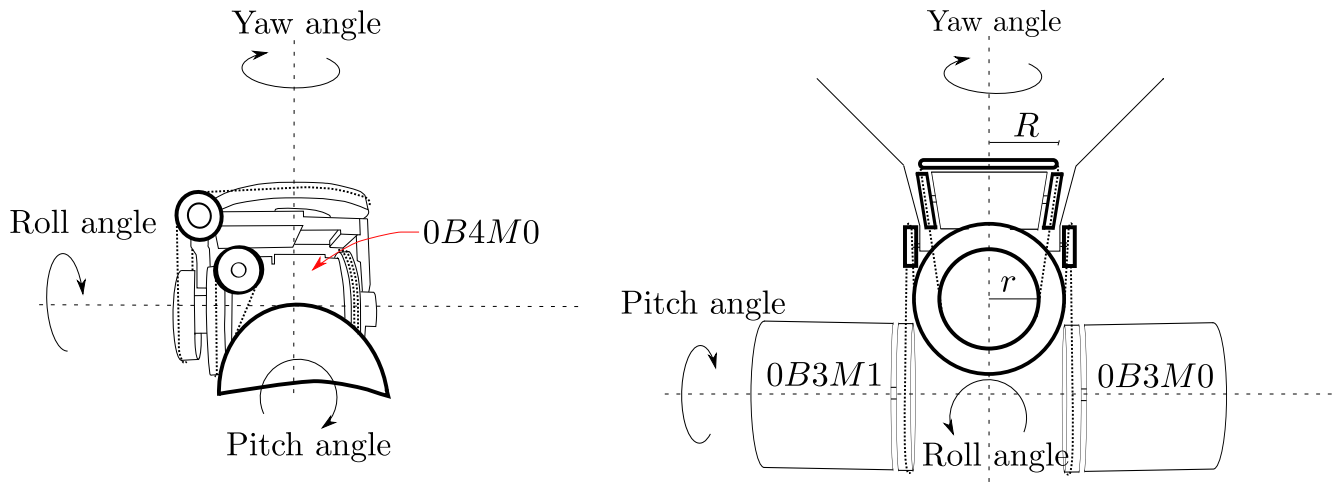
Figure 5. The sketch represents the differential joint at the iCub torso. The pitch, yaw and roll joints are actuated with three motors 0B4M0, 0B3M0, 0B3M1 in differential configuration. Motor ($\theta \in \mathbb{R}^3$) and joint ($q \in \mathbb{R}^3$) positions are coupled as described in Fig. 6.
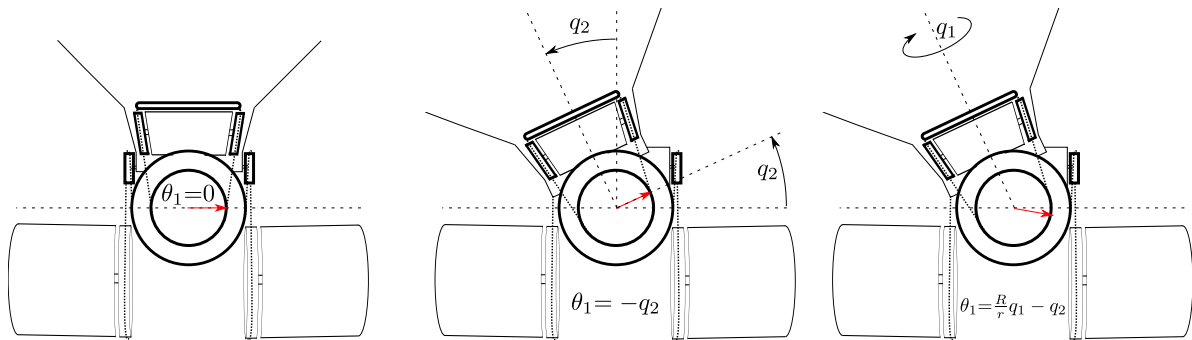

Figure 6. The sketch is used to represent the kinematic coupling between the yaw and roll movements. A roll movement of an angle q_2 implies an equal and opposite movement of the rotor of the motor 0B4M0. This rotor moves, modulo the transmission ratio, also when a yaw movement of an angle q_1 occurs.

transformations need to be applied. In the case of coupled joints, our current software [5] implements joint per joint equations (3) and (4) with substitutions $\tau \leftrightarrow \tau_\theta$ and $\dot{q} \leftrightarrow \dot{\theta}$ where motor velocity ($\dot{\theta}$) and motor torques τ_θ are obtained from joint velocity ($\dot{q}$) and joint torques (τ_q) as follows:

$$\dot{\theta} = T^{-1}\dot{q}, \qquad \tau_\theta = T^\top \tau_q.$$

3.4 COMPLETE FORCE CONTROL

In this section we describe the control algorithm for controlling an articulated rigid body subject to multiple rigid constraints. The system dynamics are described by the following constrained differential equations:

---

[5] Both the identification (3) and control (4) are available with an open source license. See the documentation in `http://wiki.icub.org/codyco/dox/html/group__motorFrictionIdentification.html` and `http://wiki.icub.org/codyco/dox/html/group__codyco__jointTorqueControl.html` respectively.

$$\underbrace{\begin{bmatrix} M_b & M_{bj} \\ M_{bj}^\top & M_j \end{bmatrix}}_{M(q)} \underbrace{\begin{bmatrix} \dot{v}_b \\ \ddot{q}_j \end{bmatrix}}_{\dot{v}} + \underbrace{\begin{bmatrix} h_b \\ h_j \end{bmatrix}}_{h(q,v)} - \underbrace{\begin{bmatrix} J_{cb}^\top \\ J_{cj}^\top \end{bmatrix}}_{J_c(q)^\top} f = \underbrace{\begin{bmatrix} 0_{6\times n} \\ I_{n\times n} \end{bmatrix}}_{S^\top} \tau \tag{7a}$$

$$J_c(q)\dot{v} + \dot{J}_c(q,v)v = 0, \tag{7b}$$

400 where $q \in SE(3) \times \mathbb{R}^n$, with $SE(3)$ the special euclidian group, represents the configuration of the
401 floating base system, which is given by the pose of a base-frame (belonging to $SE(3)$) and n generalized
402 coordinates (q_j) characterizing the joint angles . Then, $v \in \mathbb{R}^{n+6}$ represents the robot velocity (it includes
403 both $\dot{q}_j \in \mathbb{R}^n$ and the floating-base linear and angular velocity $v_b \in \mathbb{R}^6$), $\dot{v}$ is the derivative of v, the
404 control input $\tau \in \mathbb{R}^n$ is the vector of joint torques, $M \in \mathbb{R}^{(n+6)\times(n+6)}$ is the mass matrix, $h \in \mathbb{R}^{n+6}$
405 contains both gravitational and Coriolis terms, $S \in \mathbb{R}^{n\times(n+6)}$ is the matrix selecting the actuated degrees
406 of freedom, $f \in \mathbb{R}^k$ is the vector obtained by stacking all contact wrenches, which implies that $k = 6N_c$
407 and N_c the number of (rigid) contacts, $J_c \in \mathbb{R}^{k\times(n+6)}$ is the contact Jacobian. Let us first recall how the
408 force-control problem is solved in the Task Space Inverse Dynamics (TSID) framework proposed by **Del**
409 **Prete** (2013) in the context of floating-base robots. The framework computes the joint torques to match
410 as close as possible a desired vector of forces at the contacts (8a) while being compatible with the system
411 dynamics (8b) and contact constraints (8c):

$$\tau^* = \arg \min_{\tau \in \mathbb{R}^n} \|f - f^*\|^2 \tag{8a}$$

$$s.t. \quad M\dot{v} + h - J_c^\top f = S^\top \tau \tag{8b}$$

$$J_c\dot{v} + \dot{J}_c v = 0 \tag{8c}$$

412 where $f^* \in \mathbb{R}^k$ is the desired value for the contact forces. Then we can exploit the null space of the force
413 task to perform $N - 1$ motion tasks at lower priorities. These tasks (indexed with $i = 1, \ldots, N - 1$) are
414 all represented as the problem of tracking a given reference acceleration $\dot{v}_i^*$ for a variable x_i differentially
415 linked to q by the Jacobian J_i as follows:

$$\dot{x}_i = J_i v, \qquad \ddot{x}_i = J_i \dot{v} + \dot{J}_i v. \tag{9}$$

416 Assuming that the force task has maximum priority the solution is:

$$\tau^* = -(J_c\bar{S})^\top f^* + N_j^{-1}\dot{v}_1^* + \bar{S}^\top n, \tag{10}$$

417 where $N_j^{-1} = M_j - M_{bj}M_j^{-1}M_{bj}^\top$, $\bar{S} = \begin{bmatrix} -M_{bj}^\top M_b^{-1} & I \end{bmatrix}^\top$ and the term $\dot{v}_1^*$ is computed solving the
418 following recursion for $i = N, \ldots, 1$:

$$\dot{v}_i = \dot{v}_{i+1} + (J_i\bar{S}N_{p(i)})^\dagger(\ddot{x}_i^* - \dot{J}_i v + J_i(U^\top M_b^{-1}(h_b - J_{cb}^\top f) - \bar{S}\dot{v}_{i+1}))$$

$$N_{p(i)} = N_{p(i+1)} - (J_{i+1}\bar{S}N_{p(i+1)})^\dagger J_{i+1}\bar{S}N_{p(i+1)}, \tag{11}$$

419 where $U \in \mathbb{R}^{6\times(n+6)}$ is the matrix selecting the floating-base variables, and the algorithm is initialized
420 setting $\dot{v}_{N+1} = 0$, $N_{p(N)} = I$, $J_N = J_c$ and $\ddot{x}_N = 0$. The implementation of this controller exploits the
421 fact that we can compute (10) with an efficient hybrid-dynamics algorithm.

4 RESULTS

4.1 SET OF ADMISSIBLE TASKS

422 The final validation of the proposed control framework requires the definition of a suitable set of position
423 ($\ddot{x}_i^*$) and wrences (w^*) tasks and their relative priority. The set of admissible tasks is quite flexible also
424 considering the flexibility of the underlying software libraries[6]. Nevertheless we list here a set of possible
425 tasks, which we will use as a reference in the following sections. Quantities are defined with a notation
426 similar to the one used by **Featherstone** (2008): H denotes the total spatial momentum of an articulated
427 rigid body (including linear and angular), w indicates a wrench (a single vector for forces and torques),
428 the index $i = 0, 1, \ldots, N_B - 1$ is used to reference the N_B rigid bodies representing the iCub body
429 chain (0 being defined as the pelvis rigid link), the index W is used to represent the world reference
430 frame, the superscripts and subscripts la, ra, lf and rf indicate reference frames rigidly attached to the
431 left arm, right arm, left foot and right foot respectively, the superscript i indicates the reference frame
432 attached to the i-th rigid body, ^kX_i represents the rigid motion vector transformation from the reference
433 frame i to the reference frame j, $^jX_i^*$ represents the force vector transformation from the reference frame
434 i to the reference frame j, q_j represents the angular position of iCub joints. Tasks will be thrown out of
435 the following set of admissible tasks. For each task T_i we specify the reference values ($\ddot{x}_i$ or w^*) and
436 associated Jacobians (J_i).

437 • T_w^{rf} : right foot wrench task. Regulate the right foot interaction wrench to a predefined value:

$$w_i^* : \quad w_{rf} = w_{rf}^*;$$
$$J_i : \quad J_{rf};$$

438 • T_w^{lf} : left foot wrench task. Regulates the left foot interaction wrench to a predefined value:

$$w_i^* : \quad w_{lf} = w_{lf}^*;$$
$$J_i : \quad J_{lf};$$

439 • T_w^{ra} : right arm wrench task. Regulate the right arm interaction wrench to a predefined value:

$$w_i^* : \quad w_{ra} = w_{ra}^*;$$
$$J_i : \quad J_{ra};$$

440 • T_w^{la} : left arm wrench task. Regulates the left arm interaction wrench to a predefined value:

$$w_i^* : \quad w_{la} = w_{la}^*;$$
$$J_i : \quad J_{la};$$

441 • T^q : postural task. Maintains the robot joints q_j close to certain reference posture q_j^*:

$$x_q^* : \quad \ddot{q}_j = \ddot{q}_j^*;$$
$$J_i : \quad I.$$

4.2 SEQUENCING OF TASKS

442 The set of tasks active at a certain instant of time is regulated by a finite state machine. In particular there
443 are five different states $S_1, \ldots, S_5$ each characterized by a different set of active tasks $\mathcal{S}_1, \ldots, \mathcal{S}_5$.

---

[6] http://wiki.icub.org/codyco/dox/html/group__iDynTree.html

444   • S_1 has the following set of active tasks $\mathcal{S}_1 = \{T^q\}$.

445   • S_2 has the following set of active tasks $\mathcal{S}_2 = \left\{T^{lf}_w, T^{rf}_w\right\} \cup \mathcal{S}_1$.

446   • S_3 has the following set of active tasks $\mathcal{S}_3 = \{T^{ra}_w\} \cup \mathcal{S}_2$.

447   • S_4 has the following set of active tasks $\mathcal{S}_4 = \{T^{la}_w\} \cup \mathcal{S}_2$.

448   • S_5 has the following set of active tasks $\mathcal{S}_5 = \left\{T^{la}_w, T^{ra}_w\right\} \cup \mathcal{S}_2$.

449   Transition between states is regulated by the following finite state machine where the sets C_{ra} and C_{la}
450   contain the taxels (tactile elements) activated at time t.

451
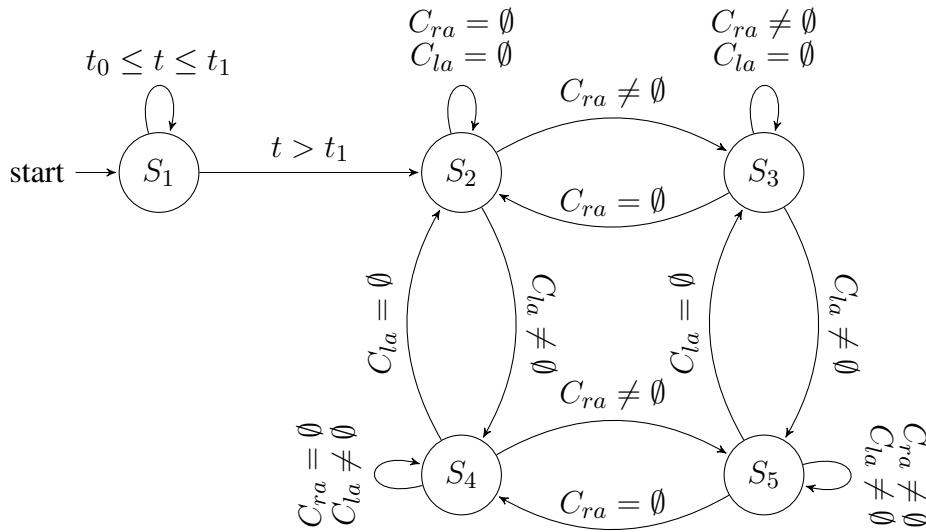
452   In practice, at start ($t = t_0$) the robot is in state S_1 in order to maintain a configuration which is as close as
453   possible to the initial configuration with a postural task (T^q) that guarantees that the system is not drifting.
454   After a predefined amount of time ($t = t_1$) the system switches to state S_2 by adding two tasks to the
455   set of active tasks: a control of the forces exchanged by the left and right foot (T^{rf}_w, T^{lf}_w respectively).
456   The control of these forces allows for a direct control over the rate of change of the momentum as will
457   be explained in Section 4.3. Successive transitions are triggered by the tactile sensors. If no contact is
458   detected on the right and left arm ($C_{ra} = \emptyset$ and $C_{ra} = \emptyset$ respectively) the system remains in S_2. A
459   transition from S_2 to S_3 is performed when the system detects a contact on the right arm ($C_{ra} \neq \emptyset$): in
460   this state the active tasks are the same active in S_2 with the addition of the task responsible for controlling
461   the force at the right arm contact location (T^{ra}_w). Similarly, a transition from S_2 to S_4 is performed when
462   the system detects a contact on the left arm ($C_{la} \neq \emptyset$): in this state the active tasks are the same active in
463   S_2 with the addition of a task responsible for controlling the force at the left arm contact location (T^{la}_w).
464   Finally a transition from either S_3 or S_4 to S_5 is performed whenever the robot perceives a contact so that
465   in this new situation both arms are in contact ($C_{ra} \neq \emptyset$ and $C_{la} \neq \emptyset$ respectively). In S_5 both arms are
466   used to control the interaction forces by activating the tasks T^{ra}_w and T^{la}_w.

4.3 TASK REFERENCES

In this section we discuss how to compute the task references:

$$w^*_{ra}, \quad w^*_{la}, \quad w^*_{rf}, \quad w^*_{lf}, \quad \ddot{q}^*_j.$$

467 to be used in the controller (8). Instantaneous values for forces are computed so as to follow a desired
468 trajectory of the center of mass (x_{com}^d) and to reduce the system's angular momentum. Instantaneous
469 values for $\ddot{q}_j^*$ are chosen so as to follow a desired reference posture q_j^d. The latter is obtained by choosing:

$$\ddot{q}_j^*(t) = \ddot{q}_j^d(t) - K_d^q\left(\dot{q}_j - \dot{q}_j^d(t)\right) - K_p^q\left(q_j - q_j{}^d(t)\right), \tag{12}$$

470 where K_p^q and K_d^q are arbitrary positive-definite matrices that take into account that in the presence
471 of modeling errors, the acceleration imposed on the system $\ddot{q}_j$ might differ from the ideal one $\ddot{q}_j^*$.
472 Instantaneous values for interaction forces are instead computed to follow a prescribed center-of-mass
473 trajectory (x_{com}^d) and to reduce angular momentum. In order to do so, a reference value $\dot{H}_{com}^*$ for the total
474 rate of change of spatial momentum (expressed at the center of mass) is computed with a strategy similar
475 to (12).

$$\dot{H}_{com}^*(t) = \dot{H}_{com}^d(t) - K_d^h\left(H_{com} - H_{com}^d(t)\right) - \begin{bmatrix} K_p^{com}\left(x_{com} - x_{com}^d(t)\right) \\ 0_{3\times 1} \end{bmatrix}, \quad H_{com}^d = \begin{bmatrix} m\dot{x}_{com}^d \\ 0_{3\times 1} \end{bmatrix} \tag{13}$$

476 where K_d^h, K_p^{com} are suitably defined gain matrices, H_{com} is the spatial momentum around the center of
477 mass, x_{com} is the center-of-mass cartesian position, x_{com}^d its desired value and m is the total mass of the
478 robot. Finally, values for $f_{ra}^*, f_{la}^*, f_{rf}^*, f_{lf}^*$ can be computed from $\dot{H}_{com}^*$ considering that the time derivative
479 of the momentum equals the resultant of forces and torques if all quantities are computed with respect to
480 the center of mass. The notation is slightly complicated due to the fact that in the different scenario states
481 $S_1, \ldots, S_5$ the meaning of f (and consequently f^*) in (8) changes. In particular we have:

$$S_2: f = \begin{bmatrix} w_{rf} \\ w_{lf} \end{bmatrix}, \quad S_3: f = \begin{bmatrix} w_{ra} \\ w_{rf} \\ w_{lf} \end{bmatrix}, \quad S_4: f = \begin{bmatrix} w_{la} \\ w_{rf} \\ w_{lf} \end{bmatrix}, \quad S_5: f = \begin{bmatrix} w_{ra} \\ w_{la} \\ w_{rf} \\ w_{lf} \end{bmatrix}, \tag{14}$$

482 In the different states, the following equations on f and $\dot{H}_{com}$ always hold:

$$S_i \quad : \quad C_{S_i} f + f_g = \dot{H}_{com}, \tag{15}$$

483 where f_g is the gravitational force and where we defined C_{S_i} to be the matrix that expresses the spatial
484 forces with respect to the center of mass:

$$
\begin{aligned}
C_{S_2} &= \begin{bmatrix} {}^{com}X_{rf}^* & {}^{com}X_{lf}^* \end{bmatrix}, \\
C_{S_3} &= \begin{bmatrix} {}^{com}X_{ra}^* & {}^{com}X_{rf}^* & {}^{com}X_{lf}^* \end{bmatrix}, \\
C_{S_4} &= \begin{bmatrix} {}^{com}X_{la}^* & {}^{com}X_{rf}^* & {}^{com}X_{lf}^* \end{bmatrix}, \\
C_{S_5} &= \begin{bmatrix} {}^{com}X_{ra}^* & {}^{com}X_{la}^* & {}^{com}X_{rf}^* & {}^{com}X_{lf}^* \end{bmatrix}.
\end{aligned}
$$

485 In literature these equations (derived from the Newton-Euler equations) have been presented in detail by
486 **Orin et al.** (2013) under the name of *centroidal dynamics*. The constraints (15) on f given $\dot{H}_{com}$ are not
487 sufficient to identify a unique solution. Additional constraints or requirements need to be imposed in order

to properly define f^* to achieve the desired momentum derivative. In order to get rid of this ambiguity, the following problem can be solved when at state S_i:

$$f^* = \arg \min_f \|f - f_0\|_W^2 \qquad \text{s.t.} \qquad C_{S_i} f + f_g = \dot{H}_{com}^*, \qquad (16)$$

where $\| \cdot \|_W$ denotes a norm weighted with the matrix $W = W^\top > 0$. The solution of this optimization is given by:

$$f^* = C_{S_i}^{\dagger W} \left(\dot{H}_{com}^* - f_g \right) + (I - C_{S_i}^{\dagger W} C_{S_i}) f_0, \qquad C_{S_i}^{\dagger W} = W^{-1} C_{S_i}^\top \left(C_{S_i} W^{-1} C_{S_i}^\top \right)^{-1}. \qquad (17)$$

This solution gives a set of desired forces f^*, which generate the desired momentum derivative $\dot{H}_{com}^*$. It is worth noting here that additional constraints should be imposed on the contact forces to guarantee contact stability. In particular, planar unilateral contacts should have an associated FRI lying in the contact support polygon (see Section 2.2.3) and forces should be maintained within the contact friction cones. Considering that these constraints can be approximated with a set of linear inequalities, adding them into (16) corresponds to transforming the problem into a quadratic program, as proposed by **de Lasa et al.** (2010). In the present implementation we follow a different strategy where stability constraints are enforced by solving (16) with a suitable choice for the reference value f_0 and weight matrix W. To ensure that reference contact forces are stable in the sense of Section 2.2.3 we express f in a reference frame whose origin coincides with the center of the maximum circle inscribed in the contact polygon. Choosing f_0 to have a null torque component penalizes solutions whose FRI is closer to the polygon borders and this penalty monotonically increases with the distance from the center of the maximum circle. Similarly, friction cones constraints are enforced by choosing the components of f_0 to be sufficiently far from the cone borders. Assuming contact plane normals to coincide with the z-axis, cone borders distance is maximized with null x and y components. If a good choice for the z-axis force components is available, it can be used in f_0. Otherwise a viable choice is also to choose $f_0 = 0$ since in most realistic situations the solution f^* is dominated by the component f_g, which is always nonzero.

4.4 EXPERIMENTAL RESULTS

We implemented the proposed control strategy on the iCub humanoid. In a first phase, the iCub was balancing with both feet on the ground plane (coplanar flat contacts). The desired center of mass position was moved left to right with a sinusoidal overimposed on its initial position $x_{com}(t_0)$ along the robot transverse axis (n):

$$x_{com}^d(t) = x_{com}(t_0) + n \cdot A \sin(2\pi f_r t) \qquad (18)$$

with $f_r = 0.15 Hz$ and $A = 0.02m$ (see Fig. 7). The reference posture $q_j{}^d(t)$ was maintained at its initial configuration $q_j{}^d(t_0)$. As previously described the desired center-of-mass acceleration was obtained by suitably choosing the forces at the contact points (in this case at the feet) as represented in Fig. 8. A video of the first phase of the experiment [7] is available for the interested reader).

In a second phase, the iCub was maintaining its center of mass at its initial position $x_{com}^d(t) \equiv x_{com}(t_0)$ and the joint reference posture $q_j{}^d(t)$ was chosen so as to move the arms toward a table in front of the robot. The controller (8) was regulated by the finite state machine described in Section 4.2. At the occurrence of contacts, forces at the arms were regulated to a predefined value f_d, which was obtained by imposing two additional constraints in solving (16): $w_{ra} = w_d$ and $w_{la} = w_d$. The force-regulation task at the arms is shown in Fig. 9 and Fig. 10, which also shows that the generation of forces at the arms does not affect the center of pressure at the feet.

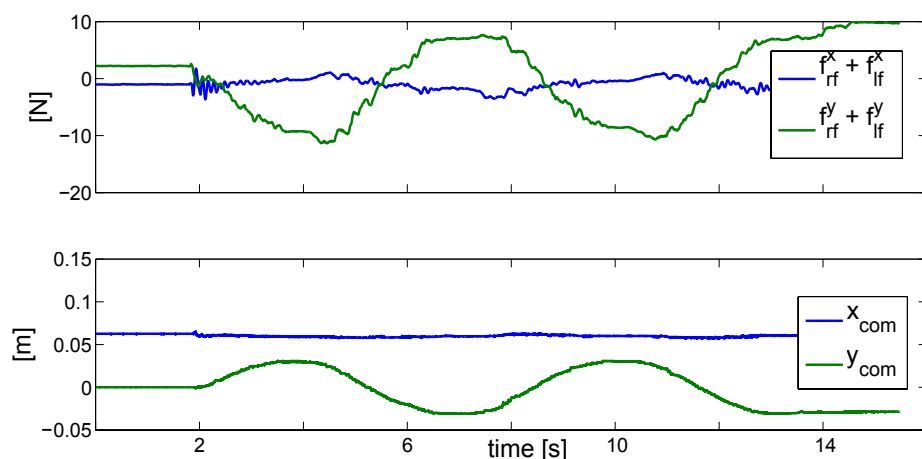[7] https://www.youtube.com/watch?v=jaTEbCsFp_M.

Figure 7. Results of the double support experiment on planar contacts (left and right feet). The picture shows the time behavior of forces (top) and center of mass position (bottom) on the sagittal (blue) and transverse (green) axis. It is worth noting that forces should be proportional to center of mass accelerations and this is visible in the plot considering that accelerations are sinusoidal in counter phase with positions. Rapid variations of the contact forces at the time $t \approx 2$, i.e. starting time, are due to the activation of the torque control.
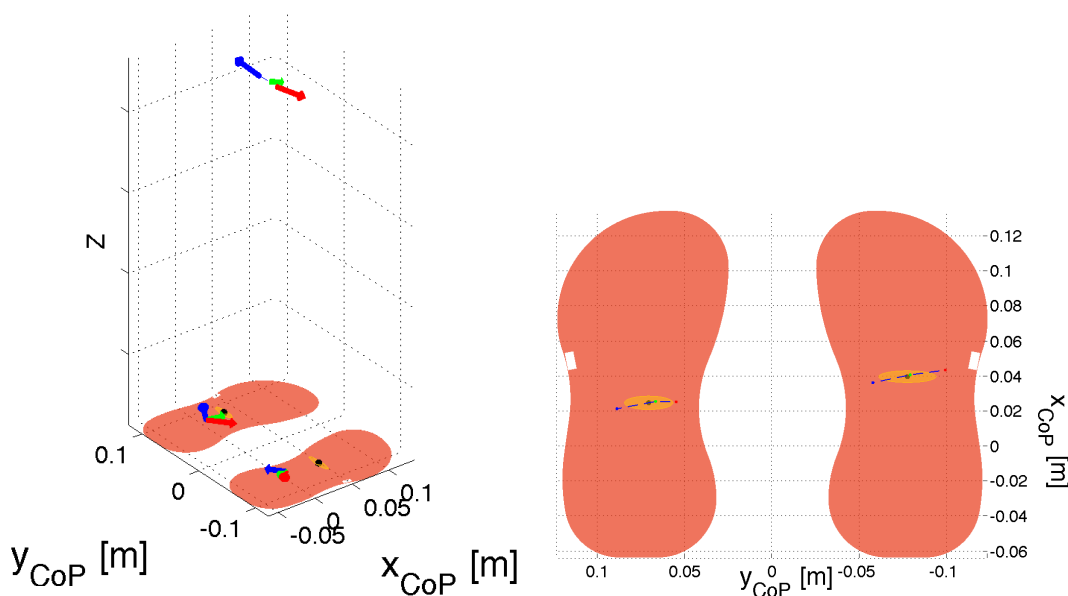

Figure 8. Results of the double support experiment on planar contacts (left and right feet). The left picture shows in three dimensions the feet contacts, the feet center of pressures, the forces at the feet and at the the center of mass during three instants: at two extrema of the sinusoid (red and blue) and in the middle of the sinusoid (green). Remarkably forces are maximum at the extrema when also accelerations are maximal. The right picture shows a close-up of of the feet with the trajectory of the center of pressure, an ellipse representing a Gaussian fit of the data points and three points corresponding to the position of the centers of pressure when at the two extrema of the sinusoid (red and blue) and in the middle of the sinusoid (green).

5 CONCLUSIONS

524   The present paper addressed the problem of whole-body motion control in the presence of multiple
525   non- coplanar and rigid contacts. The proposed solution defines a stability criterion based on the FRI
526   of individual contacts as opposed to global stability criteria. It is argued that the FRI lying on the contact
527   support polygon is a necessary and sufficient condition for the contacts to impose always the same motion
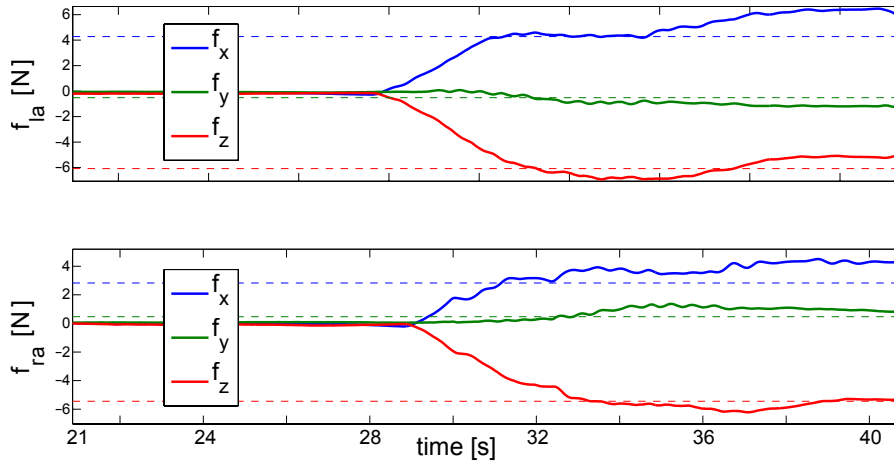
Figure 9. Results of the double support experiment on four noncoplanar contacts (both feet and arms). The plots represent the evolution of the contact forces at the left (top) and right (bottom) arms when contact is established.
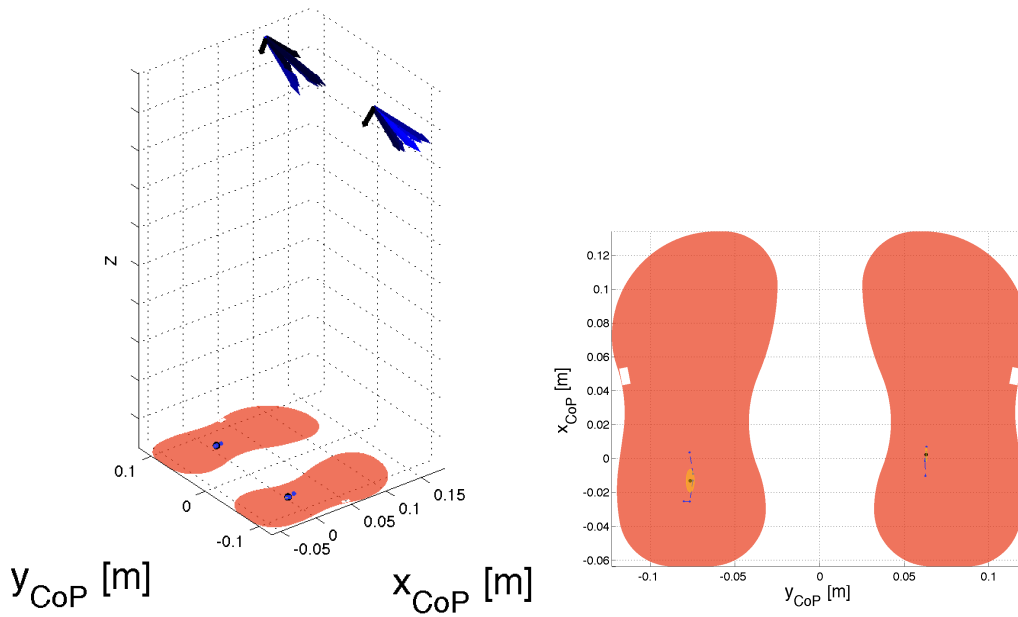

Figure 10. Results of the double-support experiment on four noncoplanar contacts (both feet and arms). The left picture gives a three-dimensional view of the foot center-of-pressure positions together with the arm contact forces. Forces are represented in a color scale that goes from black (contact establishment) to blue (steady state) . The right picture gives a closeup on the foot center-of-pressure positions with an ellipse that represents the Gaussian approximation of its distribution.

528 constraints on the whole-body dynamics. These stability conditions are therefore the ones adopted in
529 this paper in order to avoid the complications of hybrid and switching systems control. The chosen
530 stability conditions require the capability of simultaneously measuring forces and torques (i.e. wrenches)
531 at any possible contact location. This is not possible with conventional torque-controlled manipulators
532 and requires whole-body distributed force and tactile sensing. These sensing capabilities are available
533 in the iCub humanoid exploiting its whole-body distributed artificial skin and force/torque sensors. In

534 consideration of this specific hardware, in the present paper we discussed our approach to obtain: contact-
535 wrench estimates, internal-torque measurement and dynamic model identification. All these components
536 are functional to the implementation of the proposed whole-body controller with multiple noncoplanar
537 contacts.

A   COP EXISTENCE CONDITIONS

546 The Poinsot theorem (see pag. 65 in **Murray et al.** (1994)) states that every wrench applied to a rigid
547 body is equivalent to a force applied along a fixed axis plus a torque about the same axis. In particular let
548 us define a wrench (f_c^A, μ_c^A) applied at the point A. This wrench is equivalent to another wrench (f_c^L, μ_c^L)
549 applied at any point L on an axis $l = \{q' : q' = q + \lambda\omega, \quad \forall \lambda \in \mathbb{R}\}$ and whose components f_c^L and μ_c^L
550 are parallel to l, i.e. $f_c^L = \lambda_f \omega$ and $\mu_c^L = \lambda_\mu \omega$. Assuming $\|f_c^A\| \neq 0$, quantities are defined as follows:

$$\omega = \frac{f_c^A}{\|f_c^A\|}, \qquad q = \frac{f_c^A \times \mu_c^A}{\|f^A\|^2}, \qquad \lambda_f = \|f_c^A\|, \qquad \lambda_\mu = \frac{f_c^{A\top}\mu_c^A}{\|f_c^A\|}. \tag{19}$$

551 The proof of the equivalence between (f_c^A, μ_c^A) and (f_c^L, μ_c^L) is reported by **Murray et al.** (1994) and
552 therefore here omitted. In the next subsection, we prove instead that all equivalent wrenches on the Poinsot
553 axis have minimum norm torque.

A.1   POINSOT AXIS AS THE GEOMETRIC LOCUS OF MINIMUM TORQUES

554 Besides being an equivalent wrench, the Poinsot wrench (f_c^L, μ_c^L) has an associated minimum norm
555 torque μ_c^L among all equivalent wrenches. In order to prove this optimality principle, let us consider
556 the equivalent torque μ_c^Q at an arbitrary point Q:

$$\mu_c^Q = \mu_c^L + r_{QL} \times f_c^L = \lambda_\mu \omega + r_{QL} \times \lambda_f \omega, \tag{20}$$

557 being r_{QL} the vector connecting L to Q. Applying the norm to the above equation and observing that the
558 sum is an orthogonal decomposition, we obtain:

$$\|\mu_c^Q\| = \|\lambda_\mu \omega\| + \|r_{QL} \times \lambda_f \omega\| \geq \|\lambda_\mu \omega\| = \|\mu_c^L\|. \tag{21}$$

559 Therefore $\|\mu_c^Q\| \geq \|\mu_c^L\|$ and the equality holds if and only if r_{QL} is parallel to ω, i.e. when Q lies on the
560 Poinsot axis defined as:

$$\left\{ q' : q' = \frac{f_c^A \times \mu_c^A}{\|f^A\|^2} + \lambda\frac{f_c^A}{\|f_c^A\|}, \quad \forall \lambda \in \mathbb{R} \right\}. \tag{22}$$

On the Poinsot axis, the torque norm is minimal and equals:

$$\|\mu_c^{min}\| = \frac{f_c^{A\top}\mu_c^A}{\|f_c^A\|}.$$

(23)

A.2 COP EXISTENCE AND POINSOT AXIS

Given a rigid body subject to a field of pressures, the center of pressure (CoP) is an application point where the equivalent torque (due to the field of pressure) is null. Being the Poinsot axis the geometric locus of minimum torques, it is evident that a CoP can be defined if and only if $\|\mu_c^{min}\| = 0$, or equivalently if and only if f_c and μ_c are orthogonal. When this is the case, the CoP is not uniquely defined and the geometric locus of valid CoP corresponds to the Poinsot axis (22).

B COUNTEREXAMPLE ON THE GLOBAL COP AS A CONTACT STABILITY CRITERIA

In this section we provide a counterexample to show that the condition on GCoP (global center of pressure) to lie in the contacts convex hull is not sufficient to guarantee the stability of individual contacts. Consider the simple system represented in Figure 11. For certain values of the torques at the joints the global stability criteria are met (i.e. the GCoP lies in the convex hull of contacts) but individual contacts are unstable (i.e. the FRI of each contact lies outside the contact area). Given the unilateral nature of the contacts acting on the system, its solution is non-trivial and requires to make hypotheses on whether or contacts break or persist as clearly explained by **Featherstone** (2008) in chapter eleven of his book. In the specific case of Figure 11 however, it would be sufficient to just provide that particular situation in which torques at the joints force contacts to break while maintaining the GCoP within the contact support polygon. This specific situation is presented in B.3. For sake of clarity, we start with discussing the case in which contacts persist. This case just helps in understanding the proposed counterexample.

B.1 ZMP COMPUTATION

In this section we provide explicit computation for the zero tipping moment point associated to a wrench $w_c = (f_c, \mu_c)$ applied at a generic point P. It is worth stressing once more that the zero tipping moment point is by definition the ZMP, the latter name begin misleading. For sake of simpler notation, let the contact plane coincide with the x-y plane. Given the contact wrench $w_c = (f_c, \mu_c)$ at a generic point $P = [P_x, P_y, 0]$ of the contact plane, the equivalent torque μ_c' at $P' = [P_x', P_y', 0]$ is given by:

$$\mu_c' = -r_{PP'} \times f_c + \mu_c = \begin{bmatrix} \mu_c^x - r_{PP'}^y f_c^z \\ \mu_c^y + r_{PP'}^x f_c^z \\ \mu_c^z - r_{PP'}^x f_c^y + r_{PP'}^y f_c^x \end{bmatrix}$$

(24)

where $r_{PP'} = P' - P$. At a particular point P' the tipping moments along the x and y axes equal zero. This point corresponds to the zero tipping moment associated to $w_c = (f_c, \mu_c)$ and equals:

$$r_{ZMP}^x = -\frac{\mu_c^y}{f_c^z}, \qquad r_{ZMP}^y = \frac{\mu_c^x}{f_c^z}.$$

(25)

Assuming that the contact wrench $w_c = (f_c, \mu_c)$ is the resultant of a field of pressures p_c on the surface S, we have:

$$f_c^z = \int_S p_c\, dS, \qquad \mu_c^x = \int_S y p_c\, dS, \qquad \mu_c^y = \int_S -x p_c\, dS.$$
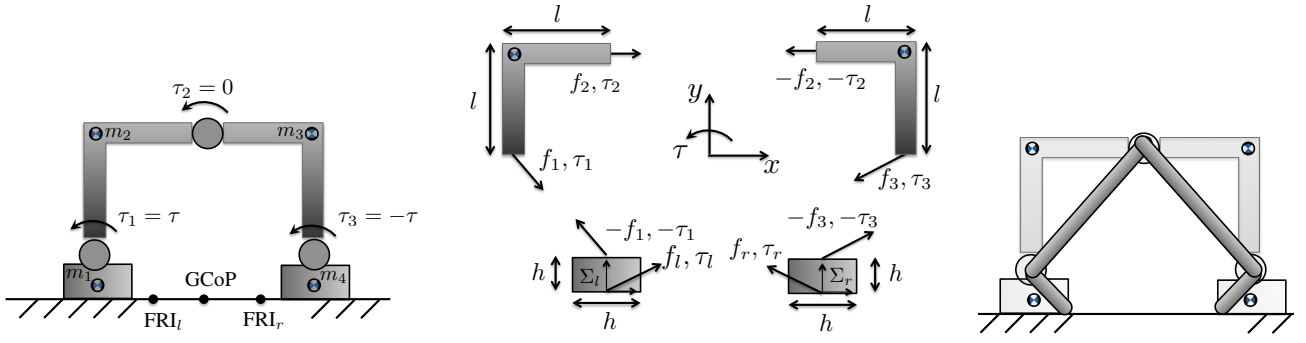
(26)

Figure 11. The image shows the example of an articulated rigid body with two links in contact with the ground. **Left figure.** The system is composed of four rigid bodies. The centers of mass associated to the rigid bodies are indicated with a check board circle. Three rotational joints have associated torques τ_1, τ_2 and τ_3. **Central figure.** The sketch shows the convention and the geometric dimension used in the computations. The contact interaction forces are indicated with $f_r, f_l \in \mathbb{R}^2$, τ_r, $\tau_l \in \mathbb{R}$; the internal constraint forces are indicated with $f_1, f_2, f_3 \in \mathbb{R}^2$. **Right figure.** The linkage that describes the system kinematic constraints when assuming that the left foot is pivoting around its right edge and the right foot around its left edge.

587 Therefore we have:

$$r^x_{\text{ZMP}} = \int_S x\alpha \, dS, \qquad r^y_{\text{ZMP}} = \int_S y\alpha \, dS, \qquad \alpha = \frac{p_c}{\int_S p_c \, dS}, \tag{27}$$

588 where in case of unilateral contacts ($p_c \geq 0$) it results evident that the ZMP is the convex combination of
589 points in S and as such it belongs to the convex hull of S.

B.2 EQUILIBRIUM CONFIGURATIONS

590 In the following paragraphs we study equilibrium configurations for the system in Fig. 11. Let us first
591 consider the case in which both contacts are active. The idea is to find conditions on the applied torques
592 to guarantee that the system is in dynamic equilibrium (i.e. null accelerations) and contacts persist. The
593 planar Newton-Euler equilibrium equations for each of the four rigid bodies composing the system give
594 twelve equations. Interaction (f_r, $f_l \in \mathbb{R}^2$, τ_r, $\tau_l \in \mathbb{R}$) and internal (f_1, f_2, $f_3 \in \mathbb{R}^2$) forces and
595 torques give twelve unknowns that can be uniquely solved for any choice of the joint torques τ_1, τ_2, τ_3.
596 To simplify the notation and to obtain a symmetric solution we assume $\tau_1 = \tau$, $\tau_2 = 0$, $\tau_3 = -\tau$. Solving
597 the associated equations gives the following solution for the contact forces:

$$f_r = \begin{bmatrix} \tau/l \\ (m_3 + m_4)g \end{bmatrix}, \qquad\qquad f_l = \begin{bmatrix} -\tau/l \\ (m_1 + m_2)g \end{bmatrix}, \tag{28a}$$

$$\tau_r = -\tau\left(1 + \frac{h}{l}\right), \qquad\qquad \tau_l = \tau\left(1 + \frac{h}{l}\right), \tag{28b}$$

598 and internal forces:

$$f_1 = \begin{bmatrix} \tau/l \\ m_2 g \end{bmatrix}, \qquad\qquad f_2 = \begin{bmatrix} \tau/l \\ 0 \end{bmatrix}, \qquad\qquad f_3 = \begin{bmatrix} -\tau/l \\ m_3 g \end{bmatrix}. \tag{29}$$

599 Assuming for the sake of simpler notation $m_1 + m_2 = m_3 + m_4 = m_{tot}/2$, (28) gives the following
600 expressions for the local right and left foot FRI[8] (expressed in the associated reference frames Σ_r and Σ_l
601 respectively):

$$\mathrm{FRI}_r = \begin{bmatrix} -\tau \frac{h+l}{mlg/2} \\ 0 \end{bmatrix}, \quad \mathrm{FRI}_l = \begin{bmatrix} \tau \frac{h+l}{mlg/2} \\ 0 \end{bmatrix}.$$

602 The global center of pressure (GCoP) can be computed by representing f_r, f_l, τ_r and τ_l in a common
603 reference frame to obtain the total force and torque f_{tot}-τ_{tot}. Using a reference frame in the middle of the
604 two contacts we have:

$$\tau_{tot}^l = \tau_r + l f_r^y + \tau_l - l f_l^y = 0, \quad f_{tot}^l = \begin{bmatrix} 0 \\ mg \end{bmatrix},$$

605 and therefore GCoP $= [0,0]^\top$. As expected by the system symmetry, the global center of pressure is
606 always in the middle of the two contacts regardless of the value given to τ. Instead, the local contacts
607 rotation indicators FRI_r and FRI_l linearly depend on τ and, for a given contact geometry, it is always
608 possible to find a τ which brings them outside the contact areas. As an example, we can assume that the
609 surfaces in contact have width $2h$ (twice the foot height) and, for sake of simpler notation $h = l/2$. With
610 this simplification the FRI is within the support polygon of each contact if and only if:

$$-\frac{mgl}{6} \leq \tau \leq \frac{mgl}{6}.$$

611 If $\tau \geq mgl/6$, the left foot rotation indicator FRI_l is on the right of the left foot support polygon. Similarly,
612 FRI_r is on the left of the right foot support polygon. In practice, recalling the results presented in Section
613 2.2, this fact implies that the computed f_r, τ_r, f_l, τ_l for the system equilibrium cannot be generated by a
614 unilateral contact of the given geometry. In a sense, the equilibrium assumption is wrong and we need to
615 redo computations with a different assumption. In the following we assume that the left foot is rotating
616 with respect to its right edge and that the right foot is rotating with respect to its left edge. We then check
617 that the solution found is feasible in terms of contact forces.

B.3 INWARD FEET ROTATION CONFIGURATIONS

618 In this section we make the hypothesis that contact constraints force the left foot to rotate around its
619 right edge and the right foot around its left edge. In this specific case the torques at the (point wise)
620 contacts are identically null. With respect to the previous situation we therefore have two unknowns less.
621 Additional unknowns come from the fact that we are no longer assuming accelerations to be identically
622 null since the system is no longer assumed at equilibrium. These additional unknowns can be expressed
623 as a function of only two unknowns (e.g. the left and right foot tipping accelerations). This results by
624 taking into consideration the kinematic constraints in the system, as represented in the left hand side
625 of Figure 11. Therefore, with respect to the equilibrium case we removed two unknowns (the torques
626 at the contacts) and inserted other two (the foot angular acceleration at the tipping point). As a result,
627 the Newton-Euler system of equations is still solvable. Deriving the solution is out of the scope of the
628 present paper and therefore omitted. The interested reader can have a look at the computations which are
629 available in MATLAB[9]. We report here the values of some important variables such as the right and left
630 foot acceleration (denoted $\ddot{q}_r$ and $\ddot{q}_l$):

---

[8] Using the FRI definition and assuming the contact plane to be $y = 0$, a force f and a torque τ have an associated FRI with x-coordinate given by $\mathrm{FRI}^x = \tau/f^y$.

[9] https://github.com/iron76/wholeBodyCounterExample

$$\ddot{q}_r = k\left(6\tau - mgl\right), \qquad \ddot{q}_l = -k\left(6\tau - mgl\right).$$

631 for some positive scalar $k > 0$ which depends only on the system geometric and dynamic parameters.
632 By convention positive accelerations correspond to counter clock wise rotations. As soon as the right foot
633 FRI starts moving away from its left edge ($\tau > mgl/6$) the right foot starts counter clock wise rotating.
634 Similarly, when the left foot FRI moves away from its right edge (again, $\tau > mgl/6$) the left foot starts
635 clock wise rotating. The left foot FRI can be computed as well. Given that the foot is not in equilibrium,
636 FRI $_l$ is computed using f_1 and τ_1 reprojected on the planar contact surface. Similar considerations hold
637 for FRI$_r$. The position of the left and right feet rotation indicators with respect to the pivoting point is
638 given by:

$$\text{FRI}_l = \frac{6\tau - mgl}{k_1 + k_2\tau}, \qquad \text{FRI}_r = -\frac{6\tau - mgl}{k_1 + k_2\tau}$$

639 where k_1 and k_2 are positive scalars which again depend only on the system geometric and dynamic
640 parameters. As expected FRI$_r$ and FRI$_l$ coincide with the pivoting point (the edge of the support polygon)
641 when $\tau = mgl/6$ and move away from the support polygon when $\tau > mgl/6$. The vertical forces at the
642 contact have the following expressions:

$$f_l^y = k_3\tau + k_4, \qquad f_r^y = k_3\tau + k_4$$

643 for positive constants k_3 and k_4. Contact forces are therefore positive as expected given the unilaterally
644 of the contact. Finally, given the symmetry of the problem, the GCoP is constantly at at the center of
645 symmetry of the system and therefore within the contact support polygon. Therefore, when $\tau > mgl/6$
646 the system starts rotating feet at their edges (contacts are broken) even if the global center of pressure is
647 within the contact convex hull. This is therefore the counterexample we were looking for.

REFERENCES

648 Aghili, F. (2005), A unified approach for inverse and direct dynamics of constrained multibody systems
649   based on linear projection operator: applications to control and simulation, *Robotics, IEEE Transactions*
650   *on*, 21, 5, 834–849
651 Ayusawa, K., Venture, G., and Nakamura, Y. (2014), Identifiability and identification of inertial
652   parameters using the underactuated base-link dynamics for legged multibody systems, *The*
653   *International Journal of Robotics Research*, 33, 3, 446–468
654 Cannata, G., Maggiali, M., Metta, G., and Sandini, G. (2008), An embedded artificial skin for humanoid
655   robots, *2008 IEEE International Conference on Multisensor Fusion and Integration for Intelligent*
656   *Systems*, 434–438
657 de Lasa, M., Mordatch, I., and Hertzmann, A. (2010), Feature-Based Locomotion Controllers, *ACM*
658   *Transactions on Graphics*, 29, 3
659 Del Prete, A. (2013), Control of Contact Forces using Whole-Body Force and Tactile Sensors: Theory
660   and Implementation on the iCub Humanoid Robot, Ph.D. thesis, Istituto Italiano di Tecnologia
661 Del Prete, A., Denei, S., Natale, L., Mastrogiovanni, F., Nori, F., Cannata, G., et al. (2011), Skin spatial
662   calibration using force/torque measurements., in IROS (IEEE), 3694–3700
663 Del Prete, A., Mansard, N., Nori, F., Metta, G., and Natale, L. (2014), Partial force control of constrained
664   floating-base robots, in Intelligent Robots and Systems, 2014. (IROS 2003). Proceedings. 2003
665   IEEE/RSJ International Conference on, –
666 Del Prete, A., Natale, L., Nori, F., and Metta, G. (2012), Contact Force Estimations Using Tactile Sensors
667   and Force / Torque Sensors, in Human-Robot Interaction (HRI), workshop on Advances in Tactile
668   Sensing and Touch based Human-Robot Interaction, Boston, USA, ACM/IEEE, 0–2

669 Featherstone, R. (2008), Rigid Body Dynamics Algorithms (Springer)

670 Fumagalli, M., Ivaldi, S., Randazzo, M., Natale, L., Metta, G., Sandini, G., et al. (2012), Force feedback
671   exploiting tactile and proximal force/torque sensing. Theory and implementation on the humanoid robot
672   iCub, *Autonomous Robots*, 33, 4, 381–398

673 Goswami, A. (1999), Postural stability of biped robots and the foot-rotation indicator (fri) point, *The
674   International Journal of Robotics Research*, 18, 6, 523–533

675 Harada, K., Kajita, S., Kaneko, K., and Hirukawa, H. (2003), Zmp analysis for arm/leg coordination,
676   in Intelligent Robots and Systems, 2003. (IROS 2003). Proceedings. 2003 IEEE/RSJ International
677   Conference on, volume 1, volume 1, 75–81 vol.1

678 Herzog, A., Righetti, L., and Grimminger, F. (2013), Experiments with a hierarchical inverse dynamics
679   controller on a torque-controlled humanoid, *arXiv preprint arXiv:1305.2042*

680 Hirai, K., Hirose, M., Haikawa, Y., and Takenaka, T. (1998), The development of honda humanoid robot,
681   in Robotics and Automation, 1998. Proceedings. 1998 IEEE International Conference on, volume 2,
682   volume 2, 1321–1326 vol.2

683 Hollerbach, J., Khalil, W., and Gautier, M. (2008), Model Identification, in B. Siciliano and O. Khatib,
684   eds., Springer Handbook of Robotics (Springer Berlin Heidelberg), 321–344

685 Huang, Q., Yokoi, K., Kajita, S., Kaneko, K., Arai, H., Koyachi, N., et al. (2001), Planning walking
686   patterns for a biped robot, *IEEE Transactions on Robotics and Automation*, 17, 280–289

687 Hyon, S.-H., Hale, J., and Cheng, G. (2007), Full-body compliant human-humanoid interaction:
688   Balancing in the presence of unknown external forces, *Robotics, IEEE Transactions on*, 23, 5, 884
689   –898

690 Kajita, S. and Espiau, B. (2008), Legged robots, in B. Siciliano and O. Khatib, eds., Springer Handbook
691   of Robotics, volume C (Springer Berlin Heidelberg), chapter 16, 361–389

692 Khatib, O. (1987), A unified approach for motion and force control of robot manipulators: The operational
693   space formulation, *IEEE Journal on Robotics and Automation*, 3, 1, 43–53

694 Li, Q., Takanishi, A., and Kato, I. (1993), Learning control for a biped walking robot with a trunk,
695   in Intelligent Robots and Systems '93, IROS '93. Proceedings of the 1993 IEEE/RSJ International
696   Conference on, volume 3, volume 3, 1771–1777 vol.3

697 Maiolino, P., Maggiali, M., Cannata, G., Metta, G., and Natale, L. (2013), A Flexible and Robust Large
698   Scale Capacitive Tactile Sensor for Robots, *IEEE Sensors Journal*

699 Metta, G., Natale, L., Nori, F., Sandini, G., Vernon, D., Fadiga, L., et al. (2010), The iCub humanoid
700   robot: an open-systems platform for research in cognitive development., *Neural Networks*, 23, 8-9,
701   1125–1134

702 Murray, R. M., Sastry, S. S., and Zexiang, L. (1994), A Mathematical Introduction to Robotic
703   Manipulation (CRC Press, Inc., Boca Raton, FL, USA), 1st edition

704 Orin, D. E., Goswami, A., and Lee, S.-H. (2013), Centroidal dynamics of a humanoid robot., *Auton.
705   Robots*, 35, 2-3, 161–176

706 Ott, C., Roa, M. a., and Hirzinger, G. (2011), Posture and balance control for biped robots based on
707   contact force optimization, *2011 11th IEEE-RAS International Conference on Humanoid Robots*, 26–
708   33, doi:10.1109/Humanoids.2011.6100882

709 Park, J. (2006), Control strategies for robots in contact, Ph.D. thesis, Stanford

710 Popovic, M. B. and Herr, H. (2005), Ground reference points in legged locomotion: Definitions, biological
711   trajectories and control implications, *Int. J. Robot. Res*, 24, 2005

712 Randazzo, M., Fumagalli, M., Nori, F., Natale, L., Metta, G., and Sandini, G. (2011), A comparison
713   between joint level torque sensing and proximal F/T sensor torque estimation: implementation on the
714   iCub, in Intelligent Robots and Systems (IROS), 2011 IEEE/RSJ International Conference on (IEEE),
715   4161–4167

716 Righetti, L., Buchli, J., Mistry, M., and Schaal, S. (2011), Control of legged robots with optimal
717   distribution of contact forces, *2011 11th IEEE-RAS International Conference on Humanoid Robots*,
718   318–324

719 Sardain, P. and Bessonnet, G. (2004), Forces Acting on a Biped Robot. Center of Pressure—Zero Moment
720   Point, *IEEE Transactions on Systems, Man, and Cybernetics - Part A: Systems and Humans*, 34, 5,
721   630–637, doi:10.1109/TSMCA.2004.832811

722 Sentis, L. (2007), Synthesis and control of whole-body behaviors in humanoid systems, Ph.D. thesis,
723   Stanford University
724 Spong, M. W. (1994), The control of underactuated mechanical systems, *First international conference*
725   *on mechatronics*
726 Stonier, D. and Kim, J.-H. (2006), Zmp analysis for realisation of humanoid motion on complex
727   topologies, in Systems, Man and Cybernetics, 2006. SMC '06. IEEE International Conference on,
728   volume 1, volume 1, 247–252, doi:10.1109/ICSMC.2006.384390
729 Vukobratovic, M. and Borovac, B. (2004), Zero-moment point - thirty five years of its life., *I. J. Humanoid*
730   *Robotics*, 1, 1, 157–173
731 Vukobratovic, M. and Juricic, D. (1969), Contribution to the synthesis of biped gait, *Biomedical*
732   *Engineering, IEEE Transactions on*, BME-16, 1, 1–6
733 Wieber, P.-B. (2002), On the stability of walking systems, in Proceedings of the International Workshop
734   on Humanoid and Human Friendly Robotics, –

FIGURES

735 **Figure 1.** Enter the caption for your figure here. Repeat as necessary for each of your figures.